7-18-2006

Magnetic instabilities and phase diagram of the double-exchange model in infinite dimensions

R. S. Fishman
Oak Ridge National Laboratory

F. Popescu
Florida State University

G. Alvarez
Oak Ridge National Laboratory

J. Moreno
University of North Dakota

Th Maier
Oak Ridge National Laboratory

See next page for additional authors

Recommended Citation

Fishman, R., Popescu, F., Alvarez, G., Moreno, J., Maier, T., & Jarrell, M. (2006). Magnetic instabilities and phase diagram of the double-exchange model in infinite dimensions. *New Journal of Physics, 8* https://doi.org/10.1088/1367-2630/8/7/116

OPEN ACCESS

Magnetic instabilities and phase diagram of the double-exchange model in infinite dimensions

New Journal of Physics
The open-access journal for physics

Magnetic instabilities and phase diagram of the double-exchange model in infinite dimensions

R S Fishman[1], F Popescu[2], G Alvarez[3], J Moreno[4], Th Maier[3] and M Jarrell[5]

[1] Materials Science and Technology Division, Oak Ridge National Laboratory, Oak Ridge, TN 37831-6032, USA
[2] Physics Department, Florida State University, Tallahassee, FL 32306, USA
[3] Computer Science and Mathematics Division, Oak Ridge National Laboratory, Oak Ridge, TN 37831-6032, USA
[4] Physics Department, University of North Dakota, Grand Forks, ND 58202-7129, USA
[5] Department of Physics, University of Cincinnati, Cincinnati, OH 45221, USA
E-mail: fishmanrs@ornl.gov

New Journal of Physics **8** (2006) 116
Received 11 April 2006
Published 18 July 2006
Online at http://www.njp.org/
doi:10.1088/1367-2630/8/7/116

Abstract. Dynamical mean-field theory is used to study the magnetic instabilities and phase diagram of the double-exchange (DE) model with Hund's coupling $J_H > 0$ in infinite dimensions. In addition to ferromagnetic (FM) and antiferromagnetic (AF) phases, the DE model also supports a broad class of short-range ordered (SRO) states with extensive entropy and short-range magnetic order. For any site on the Bethe lattice, the correlation parameter q of an SRO state is given by the average $q = \langle \sin^2(\theta_i/2) \rangle$, where θ_i is the angle between any spin and its neighbours. Unlike the FM ($q = 0$) and AF ($q = 1$) transitions, the transition temperature of an SRO state with $0 < q < 1$ cannot be obtained from the magnetic susceptibility. But a solution of the coupled Green's functions in the weak-coupling limit indicates that an SRO state always has a higher transition temperature than the AF for all fillings p below 1 and even has a higher transition temperature than the FM for $0.26 \leqslant p \leqslant 0.39$. For $0.39 < p < 0.73$, where both the FM and AF phases are unstable for small J_H, an SRO phase has a nonzero transition temperature except close to $p = 0.5$. As J_H increases, the SRO transition temperature eventually vanishes and the FM phase dominates the phase diagram. For small J_H, the $T = 0$ phase diagram of the DE model is greatly simplified by

PII: S1367-2630(06)22755-1

the presence of the SRO phase. An SRO phase is found to have lower energy than either the FM or AF phases for $0.26 \leqslant p < 1$. Phase separation (PS) disappears as $J_H \to 0$ but appears for any nonzero coupling. For fillings near $p = 1$, PS occurs between an AF with $p = 1$ and either an SRO or a FM phase. The stability of an SRO state at $T = 0$ can be understood by examining the interacting density-of-states, which is gapped for any nonzero J_H in an AF but only when J_H exceeds a critical value in an SRO state.

Contents

1. Introduction

With the renewed interest in manganites [1] and the revitalized study of dilute magnetic semiconductors [2], attention has once again focused on the double-exchange (DE) model and its variants. Applied to the manganites, the DE model is customarily formulated with one local moment per site and a Hund's coupling J_H taken to be much larger than the electron bandwidth W. In studies of dilute magnetic semiconductors, on the other hand, the local moments are sparse and the exchange coupling is comparable to W. While the full phase diagram of the DE model as a function of J_H and electron filling p has been studied by several authors [3]–[6], the properties of the DE model for small coupling constant remain very much in doubt. In particular, there have been conflicting claims about the presence of phase separation (PS) [5] and incommensurate phases [3, 4, 6] for small J_H, when the ordered ferromagnetic (FM)

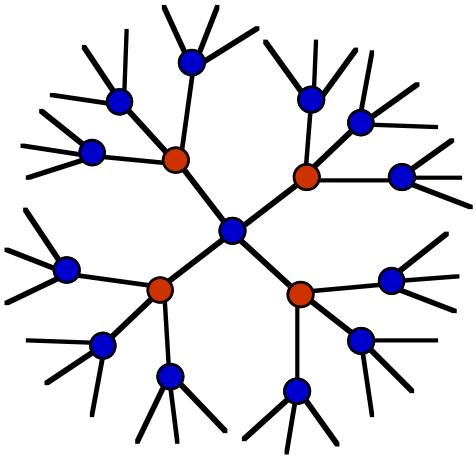

Figure 1. A Bethe lattice with $z_c = 4$ nearest neighbours. As shown, the Bethe lattice may be partitioned into A and B sublattices, denoted by the blue and red dots.

and antiferromagnetic (AF) phases are magnetically frustrated by a Ruderman–Kittel–Kasuya–Yosida (RKKY)-like interaction between the local moments [7].

This paper uses dynamical mean-field theory (DMFT) to evaluate the magnetic instabilities and $T = 0$ phase diagram of the DE model. Developed in the late 1980s by Müller-Hartmann [8] and Metzner and Vollhardt [9], DMFT exploits the momentum-independence of the self-energy in infinite dimensions, where DMFT becomes formally exact. Even in three dimensions, DMFT is believed to capture the physics of correlated systems including the narrowing of electron bands and the Mott–Hubbard transition [10]. Although DMFT has been widely applied to the DE model [4, 5], [11]–[18], until now there has been no complete treatment of the phase instabilities and $T = 0$ phase diagram of the DE model for arbitrary J_H and p.

We shall study a system with a bare semicircular density-of-states (DOS) given by $N_0(\omega) = (8/\pi W^2)\mathrm{Re}\sqrt{W^2/4 - \omega^2}$. In real space, this DOS belongs to an infinite-dimensional Bethe lattice or an infinite Cayley tree with no closed loops [19]. A finite-dimensional Bethe lattice with coordination number $z_c = 4$ is sketched in figure 1. Although the Bethe lattice lacks translational symmetry, it is quite convenient for calculations. As shown in figure 1, the Bethe lattice can be partitioned into A and B sublattices so that both FM and AF long-range orders are possible. Due to the bounds $\pm W/2$, the DOS of the Bethe lattice more closely resembles the DOS of two- and three-dimensional systems than does the unbounded DOS of the hypercubic lattice. Indeed, pathological results have been obtained on a hypercubic lattice due to the asymptotic freedom of the quasiparticles in the tails of the Gaussian DOS [16]. As we shall see, the Bethe lattice also has the advantage that analytic results are possible in the limit of small J_H, precisely the regime where controversies persist.

The high-temperature, non-magnetic (NM) phases of the Heisenberg and DE models have a correlation length ξ that vanishes as $z_c \to \infty$. By contrast, the short-range ordered (SRO) states introduced in an earlier paper [20] possess some of the same characteristics as spin glasses: local magnetic order and exponentially decaying magnetic correlations [21]. The SRO states are characterized by the correlation parameter $q = \langle \sin^2(\theta_i/2)\rangle$, where θ_i are the angles between any spin and its neighbours. Overall, the neighbouring spins describe a cone with angle $2\arcsin(\sqrt{q})$

around the central spin. This disordered state reduces to the FM and AF phases when $q = 0$ and 1 respectively. Unlike the FM and AF phases, an SRO state with $0 < q < 1$ has extensive entropy and short-range but not long-range magnetic order. Since it is not possible to associate a wavevector with any SRO state, its transition temperatures $T_{\mathrm{SRO}}(p, q)$ cannot be obtained from the magnetic susceptibility. Rather, $T_{\mathrm{SRO}}(p, q)$ can be solved from coupled Green's function equations. Remarkably, an SRO state can be found with higher transition temperature and lower energy than the ordered FM and AF phases in a large region of phase space.

The FM and AF transition temperatures may be obtained by solving either the coupled Green's function equations or the Bethe–Salpeter (BS) equations for the magnetic susceptibility. The BS equations break up into separate relations for the charge and spin degrees of freedom. The vertex functions of the BS equations are consistent with the functional derivative of the self-energy with respect to the Green's function [17]. It follows that the DMFT treatment of the DE model is Φ-derivable and hence thermodynamically consistent [22], meaning that identical results are obtained from both ways of evaluating T_{C} and T_{N}.

This paper is divided into seven main sections. In section 2, we formulate the BS equations for the susceptibility and derive the vertex functions. The thermodynamic consistency of the DMFT of the DE model is discussed in section 3. The BS equations are used in section 4 to derive implicit expressions for the FM and AF transition temperatures. Using coupled Green's functions, we rederive the transition temperatures of the ordered phases and evaluate the transition temperature of the SRO states. We also explicitly solve those relations in the weak-coupling limit of small J_{H}. A complete map of the phase instabilities of the DE model is provided in section 5. In section 6, we present the $T = 0$ phase diagram of the DE model both with and without the SRO states. Finally, section 7 contains a summary and conclusion. Appendix A provides results for the transition temperatures and $T = 0$ energies of the SRO states in the weak-coupling limit. In appendix B, we derive the self-consistency relation for the SRO states. Appendix C provides a convenient and general form for the kinetic energy of the SRO and ordered phases.

2. BS equations and the vertex functions

The Hamiltonian of the DE model (also called the FM Kondo model when $J_{\mathrm{H}} < \infty$) is given by

$$H = -t \sum_{\langle i,j \rangle} \left(c^{\dagger}_{i\alpha} c_{j\alpha} + c^{\dagger}_{j\alpha} c_{i\alpha} \right) - 2J_{\mathrm{H}} \sum_{i} \mathbf{s}_i \cdot \mathbf{S}_i, \tag{1}$$

where $c^{\dagger}_{i\alpha}$ and $c_{i\alpha}$ are the creation and destruction operators for an electron with spin α at site i, $J_{\mathrm{H}} > 0$ is the Hund's coupling, $\mathbf{s}_i = c^{\dagger}_{i\alpha} \sigma_{\alpha\beta} c_{i\beta}/2$ is the electronic spin, and $\mathbf{S}_i = S\mathbf{m}_i$ is the spin of the local moment. Repeated spin indices are summed. The local moment will be treated classically, which is only a fair approximation for the magnanites with spin $S = 3/2$ but a better approximation for dilute magnetic semiconductors with $S = 5/2$. For large z_{c}, the hopping energy t scales as $1/\sqrt{z_{\mathrm{c}}}$ and the local effective action on site 0 may be written [11]

$$S_{\mathrm{eff}}(\mathbf{m}) = -T \sum_{n} \bar{c}_{0\alpha}(\mathrm{i}\nu_n) \{ G_0(\mathrm{i}\nu_n)^{-1}_{\alpha\beta} + J\sigma_{\alpha\beta} \cdot \mathbf{m} \} c_{0\beta}(\mathrm{i}\nu_n), \tag{2}$$

where $J = J_{\mathrm{H}} S$, $\nu_n = (2n+1)\pi T$, $\bar{c}_{0\alpha}(\mathrm{i}\nu_n)$ and $c_{0\alpha}(\mathrm{i}\nu_n)$ are now anticommuting Grassman variables, $\mathbf{m}$ is the orientation of the local moment on site 0, and $\underline{G}_0(\mathrm{i}\nu_n)$ is the bare Green's

function containing dynamical information about the hopping of electrons from other sites onto site 0 and off again.

Because $S_{\rm eff}(\mathbf{m})$ is quadratic in the Grassman variables, the full Green's function $\mathcal{G}(\mathbf{m}, \mathrm{i}\nu_n)_{\alpha\beta}$ at site 0 for a fixed $\mathbf{m}$ may be readily solved by integrating over the Grassman variables, with the NM result

$$\underline{\mathcal{G}}(\mathbf{m}, \mathrm{i}\nu_n) = \{G_0(\mathrm{i}\nu_n)^{-1}\underline{I} + J\underline{\sigma}\cdot\mathbf{m}\}^{-1} = \frac{G_0(\mathrm{i}\nu_n)^{-1}\underline{I} - J\underline{\sigma}\cdot\mathbf{m}}{G_0(\mathrm{i}\nu_n)^{-2} - J^2}, \tag{3}$$

where $G_0(\mathrm{i}\nu_n)_{\alpha\beta} = \delta_{\alpha\beta}G_0(\mathrm{i}\nu_n)$ is diagonal above $T_{\rm C}$. Averaging over the orientations of the local moment, $\langle\mathcal{G}(\mathbf{m}, \mathrm{i}\nu_n)_{\alpha\beta}\rangle_{\mathbf{m}} = G(\mathrm{i}\nu_n)_{\alpha\beta} = \delta_{\alpha\beta}G(\mathrm{i}\nu_n)$ where

$$G(\mathrm{i}\nu_n) = \frac{G_0(\mathrm{i}\nu_n)^{-1}}{G_0(\mathrm{i}\nu_n)^{-2} - J^2}. \tag{4}$$

If $P(\mathbf{m}) = \mathrm{Tr}_{\rm f}(\exp(-S_{\rm eff}(\mathbf{m}))/Z$ is the probability for the local moment to point in the $\mathbf{m}$ direction, then the average over $\mathbf{m}$ is given by $\langle C(\mathbf{m})\rangle_{\mathbf{m}} \equiv \int \mathrm{d}\Omega_{\mathbf{m}}\, P(\mathbf{m})C(\mathbf{m})$. The effective partition function Z involves both a trace over the Fermion degrees of freedom and an average over $\mathbf{m}$: $Z = \int \mathrm{d}\Omega_{\mathbf{m}}\,\mathrm{Tr}_{\rm f}(\exp(-S_{\rm eff}(\mathbf{m})))$. Above $T_{\rm C}$, $P(\mathbf{m}) = 1/4\pi$ is constant. Consequently, the NM self-energy is $\Sigma(\mathrm{i}\nu_n) = G_0(\mathrm{i}\nu_n)^{-1} - G(\mathrm{i}\nu_n)^{-1} = J^2G_0(\mathrm{i}\nu_n)$.

Likewise above $T_{\rm C}$, the lattice Green's function $\mathcal{G}(\mathbf{m}, \mathbf{k}, \mathrm{i}\nu_n)_{\alpha\beta}$ has the expectation value

$$\langle\mathcal{G}(\mathbf{m}, \mathbf{k}, \mathrm{i}\nu_n)_{\alpha\beta}\rangle_{\mathbf{m}} = \delta_{\alpha\beta}\frac{1}{z_n - \epsilon_{\mathbf{k}} - J^2G_0(\mathrm{i}\nu_n)} \tag{5}$$

with $z_n = \mathrm{i}\nu_n + \mu$. Summing equation (5) over all $\mathbf{k}$ and equating the result to equation (4), we obtain [10, 11]

$$G_0(\mathrm{i}\nu_n)^{-1} = z_n - \frac{W^2}{16}G(\mathrm{i}\nu_n), \tag{6}$$

where $W = 4t\sqrt{z_{\rm c}}$ is the full bandwidth of the semi-circular DOS.

Our goal is to evaluate the general susceptibility [15]

$$\sum_{l,n}\chi^{\beta\alpha,\delta\kappa}_{\mathbf{q},\mathrm{i}\omega_m}(\mathrm{i}\nu_l, \mathrm{i}\nu_n) = \int_0^\beta \mathrm{d}\tau\, \mathrm{e}^{\mathrm{i}\omega_m\tau}\sum_i \mathrm{e}^{-\mathrm{i}\mathbf{q}\cdot(\mathbf{R}_i-\mathbf{R}_0)}\{\langle T_\tau c^\dagger_{i\alpha}(\tau)c_{i\beta}(\tau)c^\dagger_{0\kappa}c_{0\delta}\rangle - \langle c^\dagger_{i\alpha}c_{i\beta}\rangle\langle c^\dagger_{0\kappa}c_{0\delta}\rangle\}, \tag{7}$$

where $\omega_m = 2m\pi T$ and $\langle C\rangle$ involves both a Fermion trace and an average over all the $\mathbf{m}_i$. Sketched in figures 1(a) and (b), the general susceptibility and the full vertex function $\Gamma^{\eta\mu,\tau\nu}_{\mathrm{i}\omega_m}(\mathrm{i}\nu_l, \mathrm{i}\nu_n)$ are related by the lattice BS equation:

$$\underline{\chi}^{\beta\alpha,\delta\kappa}_{\mathbf{q},\mathrm{i}\omega_m} = \underline{\chi}^{(0)\beta\alpha,\delta\kappa}_{\mathbf{q},\mathrm{i}\omega_m} + \underline{\chi}^{(0)\beta\alpha,\mu\eta}_{\mathbf{q},\mathrm{i}\omega_m}\underline{\Gamma}^{\eta\mu,\tau\nu}_{\mathrm{i}\omega_m}\underline{\chi}^{\nu\tau,\delta\kappa}_{\mathbf{q},\mathrm{i}\omega_m}. \tag{8}$$

Each term in this equation is a matrix in Matsubara space and matrix multiplication involves a summation over intermediate Matsubara frequencies, as shown in figure 2(c) [15]. The local susceptibility $\underline{\chi}^{\beta\alpha,\delta\kappa}_{\mathrm{i}\omega_m}$ is obtained from the lattice susceptibility $\underline{\chi}^{\beta\alpha,\delta\kappa}_{\mathbf{q},\mathrm{i}\omega_m}$ by summing over $\mathbf{q}$ and

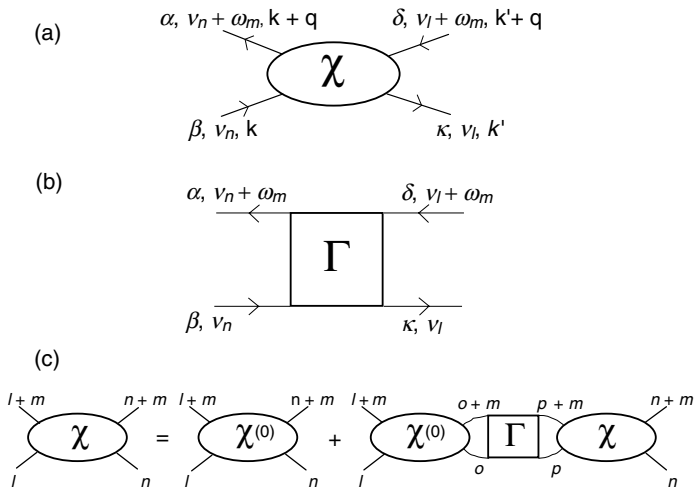

Figure 2. Diagrammatic representations of (a) the magnetic susceptibility $\chi^{\beta\alpha,\delta\kappa}_{\mathbf{q},\mathrm{i}\omega_m}(\mathrm{i}\nu_l, \mathrm{i}\nu_n)$, (b) the vertex function $\Gamma^{\beta\alpha,\delta\kappa}_{\mathrm{i}\omega_m}(\mathrm{i}\nu_l, \mathrm{i}\nu_n)$ and (c) the BS equations.

satisfies the local BS equation:

$$\underline{\chi}^{\beta\alpha,\delta\kappa}_{\mathrm{i}\omega_m} = \underline{\chi}^{(0)\beta\alpha,\delta\kappa}_{\mathrm{i}\omega_m} + \underline{\chi}^{(0)\beta\alpha,\mu\eta}_{\mathrm{i}\omega_m} \underline{\Gamma}^{\eta\mu,\tau\nu}_{\mathrm{i}\omega_m} \underline{\chi}^{\nu\tau,\delta\kappa}_{\mathrm{i}\omega_m}. \tag{9}$$

Since the vertex function is independent of momentum in infinite dimensions, it appears identically in both the lattice and local BS equations [23, 24].

For the bare susceptibilities, the electrons in each Green's function are uncorrelated, which means that each Green's function is separately averaged over **m**. So the bare lattice susceptibility is given by

$$\chi^{(0)\beta\alpha,\delta\kappa}_{\mathbf{q},\mathrm{i}\omega_m}(\mathrm{i}\nu_l, \mathrm{i}\nu_n) = -\frac{T}{N}\delta_{ln}\sum_{\mathbf{k}} \langle \mathcal{G}(\mathbf{m}, \mathbf{k}, \mathrm{i}\nu_l)_{\alpha\delta}\rangle_{\mathbf{m}} \langle \mathcal{G}(\mathbf{m}, \mathbf{k}+\mathbf{q}, \mathrm{i}\nu_{l+m})_{\kappa\beta}\rangle_{\mathbf{m}}. \tag{10}$$

The bare local susceptibility is obtained by summing this expression over all **q**:

$$\chi^{(0)\beta\alpha,\delta\kappa}_{\mathrm{i}\omega_m}(\mathrm{i}\nu_l, \mathrm{i}\nu_n) = -T\delta_{ln} G(\mathrm{i}\nu_l)_{\alpha\delta} G(\mathrm{i}\nu_{l+m})_{\kappa\beta}, \tag{11}$$

where $G(\mathrm{i}\nu_l)_{\alpha\beta} = \delta_{\alpha\beta}G(\mathrm{i}\nu_l)$ is the **m**-averaged local Green's function given by equation (4). It is also straightforward to evaluate the full local susceptibility:

$$\begin{aligned}\chi^{\beta\alpha,\delta\kappa}_{\mathrm{i}\omega_m}(\mathrm{i}\nu_l, \mathrm{i}\nu_n) = T\delta_{m,0}\left\{\langle \mathcal{G}(\mathbf{m}, \mathrm{i}\nu_n)_{\beta\alpha}\mathcal{G}(\mathbf{m}, \mathrm{i}\nu_l)_{\delta\kappa}\rangle_{\mathbf{m}} - \langle \mathcal{G}(\mathbf{m}, \mathrm{i}\nu_n)_{\beta\alpha}\rangle_{\mathbf{m}}\langle \mathcal{G}(\mathbf{m}, \mathrm{i}\nu_l)_{\delta\kappa}\rangle_{\mathbf{m}}\right\} \\ -T\delta_{ln}\langle \mathcal{G}(\mathbf{m}, \mathrm{i}\nu_l)_{\alpha\delta}\mathcal{G}(\mathbf{m}, \mathrm{i}\nu_{l+m})_{\kappa\beta}\rangle_{\mathbf{m}},\end{aligned} \tag{12}$$

where $\mathcal{G}(\mathbf{m}, \mathrm{i}\nu_l)_{\alpha\beta}$ is the **m**-dependent local Green's function given by equation (3).

Due to the matrix structure of equations (10)–(12), the charge and spin degrees of freedom decouple: $\sigma^{\alpha\beta}_z \underline{\chi}^{(0)\beta\alpha,\delta\kappa}_{\mathbf{q},\mathrm{i}\omega_m} \propto \sigma^{\delta\kappa}_z$ and $\delta^{\alpha\beta}\underline{\chi}^{(0)\beta\alpha,\delta\kappa}_{\mathbf{q},\mathrm{i}\omega_m} \propto \delta^{\delta\kappa}$ with analogous relations for the local susceptibilities. We define the charge and spin susceptibilities and vertex functions by $\underline{\chi}^{c}_{\mathbf{q},\mathrm{i}\omega_m} = \delta_{\alpha\beta}\underline{\chi}^{\beta\alpha,\delta\kappa}_{\mathbf{q},\mathrm{i}\omega_m}\delta_{\kappa\delta}/4$, $\underline{\chi}^{s}_{\mathbf{q},\mathrm{i}\omega_m} = \sigma^z_{\alpha\beta}\underline{\chi}^{\beta\alpha,\delta\kappa}_{\mathbf{q},\mathrm{i}\omega_m}\sigma^z_{\kappa\delta}/4$, $\underline{\Gamma}^{c}_{\mathrm{i}\omega_m} = \delta_{\alpha\beta}\underline{\Gamma}^{\beta\alpha,\delta\kappa}_{\mathbf{q},\mathrm{i}\omega_m}\delta_{\kappa\delta}$, and $\underline{\Gamma}^{s}_{\mathrm{i}\omega_m} = \sigma^z_{\alpha\beta}\underline{\Gamma}^{\beta\alpha,\delta\kappa}_{\mathbf{q},\mathrm{i}\omega_m}\sigma^z_{\kappa\delta}$. Similar definitions are employed for the local susceptibilities. Since equations (10) and (11)

imply that the bare, charge and spin susceptibilities are identical, we shall dispense with the superscripts c and s on those quantities.

After this decoupling, both the lattice and local BS equations separate into two sets of equations for the charge and spin degrees of freedom:

$$\underline{\chi}^{a}_{\mathbf{q},\mathrm{i}\omega_m} = \underline{\chi}^{(0)}_{\mathbf{q},\mathrm{i}\omega_m} + \underline{\chi}^{(0)}_{\mathbf{q},\mathrm{i}\omega_m}\underline{\Gamma}^{a}_{\mathrm{i}\omega_m}\underline{\chi}^{a}_{\mathbf{q},\mathrm{i}\omega_m}, \tag{13}$$

$$\underline{\chi}^{a}_{\mathrm{i}\omega_m} = \underline{\chi}^{(0)}_{\mathrm{i}\omega_m} + \underline{\chi}^{(0)}_{\mathrm{i}\omega_m}\underline{\Gamma}^{a}_{\mathrm{i}\omega_m}\underline{\chi}^{a}_{\mathrm{i}\omega_m}, \tag{14}$$

where $a = c$ or s. The same charge and spin vertex functions enter the lattice and local equations. The spin BS equations with $a = s$ were previously solved [15] in the strong-coupling limit $J \gg W$ and $J \gg T$.

To generally solve equation (13) for the charge and spin lattice susceptibilities, we first obtain the charge and spin vertex functions from the local susceptibilities given by equation (14). The vertex function may be written as

$$\Gamma^{\beta\alpha,\delta\kappa}_{\mathrm{i}\omega_m}(\mathrm{i}\nu_l, \mathrm{i}\nu_n) = A_{ln}\sigma_{\beta\alpha}\cdot\sigma_{\delta\kappa}\delta_{m,0} + B^{l}_{m}\sigma_{\delta\alpha}\cdot\sigma_{\beta\kappa}\delta_{ln}, \tag{15}$$

$$A_{ln} = \frac{\beta J^2}{3(1+C)}\frac{a_l a_n}{b_l b_n}, \tag{16}$$

$$B^{l}_{m} = -\frac{\beta J^2}{3}\frac{G_0(\mathrm{i}\nu_l)G_0(\mathrm{i}\nu_{l+m})a_l a_{l+m}}{G_0^{-1}(\mathrm{i}\nu_l)G_0^{-1}(\mathrm{i}\nu_{l+m}) + J^2}, \tag{17}$$

where $a_n = G_0(\mathrm{i}\nu_n)^{-2} - J^2$, $b_n = G_0(\mathrm{i}\nu_n)^{-2} - J^2/3$ and $C = -(2J^2/3)\sum_n b_n^{-1}$. In terms of A_{ln} and B^{l}_{m}, the charge and spin vertex functions are then given by $\Gamma^{c}_{\mathrm{i}\omega_m}(\mathrm{i}\nu_l, \mathrm{i}\nu_n) = 6B^{l}_{m}\delta_{ln}$ and $\Gamma^{s}_{\mathrm{i}\omega_m}(\mathrm{i}\nu_l, \mathrm{i}\nu_n) = 4A_{ln}\delta_{m,0} - 2B^{l}_{m}\delta_{ln}$.

3. Thermodynamic consistency

A thermodynamically consistent theory produces identical results from either the Green's function (which is on the single-particle level) or the partition function (which involves interactions on the two-particle level). Baym and Kadanoff [22] demonstrated that a sufficient condition for a theory to be thermodynamically consistent is that it be Φ-derivable, which means that a functional $\Phi(\{\underline{G}(\mathrm{i}\nu_n)\})$, constructed from compact diagrams involving the full Green's functions and the bare vertex functions, satisfies the condition $\Sigma(\mathrm{i}\nu_n)_{\alpha\beta} = \delta\Phi/\delta G(\mathrm{i}\nu_n)_{\alpha\beta}$. The partition function of a Φ-derivable theory satisfies the relation

$$-\log Z = \Phi - \sum_n \mathrm{Tr_f}\left\{\underline{\Sigma}(\mathrm{i}\nu_n)\underline{G}(\mathrm{i}\nu_n)\right\} + \sum_n \mathrm{Tr_f}\log\left\{\underline{G}(\mathrm{i}\nu_n)\right\}, \tag{18}$$

which is stationary under variations of $\underline{G}(\mathrm{i}\nu_n)$. Whereas Baym and Kadanoff considered systems of interacting Fermions and Bosons, their ideas were later extended to systems of interacting electrons and spins [25] and to disordered alloys [26]. The Φ-derivability of the DMFT of the DE model was first demonstrated in [17].

The bare vertex function $\Gamma^{(0)\,\beta\alpha,\delta\kappa}_{\mathrm{i}\omega_m}(\mathrm{i}\nu_l,\mathrm{i}\nu_n)$ may be associated with the two-particle interaction in the purely electronic effective action [27]

$$S'_{\mathrm{eff}} = -T\sum_n \bar{c}_{0\alpha}(\mathrm{i}\nu_n)G_0(\mathrm{i}\nu_n)^{-1}c_{0\alpha}(\mathrm{i}\nu_n) - \frac{T^3}{4}\sum_{l,n,m}\bar{c}_{0\alpha}(\mathrm{i}\nu_n+\mathrm{i}\omega_m)c_{0\beta}(\mathrm{i}\nu_n) \times\Gamma^{(0)\beta\alpha,\delta\kappa}_{\mathrm{i}\omega_m}(\mathrm{i}\nu_l,\mathrm{i}\nu_n)\bar{c}_{0\kappa}(\mathrm{i}\nu_l)c_{0\delta}(\mathrm{i}\nu_l+\mathrm{i}\omega_m). \tag{19}$$

Because the Fermion operators anticommute, the bare vertex function must satisfy the crossing symmetries $\Gamma^{(0)\,\delta\alpha,\beta\kappa}_{\mathrm{i}\omega_{n-l}}(\mathrm{i}\nu_l,\mathrm{i}\nu_{l+m}) = \Gamma^{(0)\,\beta\kappa,\delta\alpha}_{\mathrm{i}\omega_{l-n}}(\mathrm{i}\nu_{n+m},\mathrm{i}\nu_n) = -\Gamma^{(0)\,\beta\alpha,\delta\kappa}_{\mathrm{i}\omega_m}(\mathrm{i}\nu_l,\mathrm{i}\nu_n)$. There are two ways to evaluate the bare vertex function. First, we can take the $J\to 0$ limit of the full vertex function $\underline{\Gamma}^{\beta\alpha,\delta\kappa}_{\mathrm{i}\omega_m}$ given by equation (15). Alternatively, we can associate the lowest-order, J^2 contribution to the partition function $Z = \int \mathrm{d}\Omega_{\mathbf{m}}\,\mathrm{Tr}_{\mathrm{f}}(\exp(-S_{\mathrm{eff}}(\mathbf{m})))$ with the J^2 contribution to the partition function $Z' = \mathrm{Tr}_{\mathrm{f}}(\exp(-S'_{\mathrm{eff}}))$. Both methods yield the same result:

$$\underline{\Gamma}^{(0)\beta\alpha,\delta\kappa}_{\mathrm{i}\omega_m}(\mathrm{i}\nu_l,\mathrm{i}\nu_n) = \tfrac{1}{3}\beta J^2\left\{\sigma_{\beta\alpha}\cdot\sigma_{\delta\kappa}\delta_{m,0} - \sigma_{\delta\alpha}\cdot\sigma_{\beta\kappa}\delta_{ln}\right\}, \tag{20}$$

which does indeed satisfy the required crossing symmetries.

But S'_{eff} produces an inequivalent infinite-dimensional theory than produced by $S_{\mathrm{eff}}(\mathbf{m})$, as seen in the different expansions of Z and Z' to order J^4:

$$Z = Z_0\left\{1 - J^2\sum_n G_0(\mathrm{i}\nu_n)^2 + \tfrac{1}{2}J^4\sum_{l\neq n}G_0(\mathrm{i}\nu_l)^2G_0(\mathrm{i}\nu_n)^2 + \mathcal{O}(J^6)\right\}, \tag{21}$$

$$Z' = Z_0\left\{1 - J^2\sum_n G_0(\mathrm{i}\nu_n)^2 + \tfrac{5}{6}J^4\sum_{l\neq n}G_0(\mathrm{i}\nu_l)^2G_0(\mathrm{i}\nu_n)^2 + \mathcal{O}(J^6)\right\}. \tag{22}$$

Therefore, the DE action cannot be replaced by a purely electronic action containing only two-body interactions and it is not possible to construct a diagrammatic expansion in powers of $\underline{\Gamma}^{(0)}$.

Nevertheless, we can construct a functional $\Phi(\{\underline{G}(\mathrm{i}\nu_n)\})$ satisfying the condition $\Sigma(\mathrm{i}\nu_n)_{\alpha\alpha} = \delta\Phi/\delta G(\mathrm{i}\nu_n)_{\alpha\alpha}$. Starting from equation (3) and Dyson's equation for the self-energy, we obtain $\delta\Sigma(\mathrm{i}\nu_l)_{\alpha\alpha}/\delta G(\mathrm{i}\nu_n)_{\beta\beta} = (\underline{K}^{-1})^{\alpha\beta}_{ln} + \delta_{ln}\delta_{\alpha\beta}G(\mathrm{i}\nu_n)^{-2}$, where

$$K^{\alpha\beta}_{ln} = \frac{\delta G(\mathrm{i}\nu_n)_{\beta\beta}}{\delta[G_0(\mathrm{i}\nu_l)_{\alpha\alpha}]^{-1}} = -\delta_{ln}\frac{1}{a_n^2}\left\{\frac{2J^2}{3} + b_n\delta_{\alpha\beta}\right\} + \frac{J^2}{3a_la_n}(2\delta_{\alpha\beta}-1). \tag{23}$$

Inverting this Jacobian yields the general result

$$\frac{\delta\Sigma(\mathrm{i}\nu_l)_{\alpha\alpha}}{\delta G(\mathrm{i}\nu_n)_{\beta\beta}} = -\delta_{ln}\frac{J^2a_n^2}{3b_n}\left\{\frac{2}{2a_n-3b_n} + \delta_{\alpha\beta}G_0(\mathrm{i}\nu_n)^2\right\} - \frac{J^2}{3(1+C)}\frac{a_la_n}{b_lb_n}(2\delta_{\alpha\beta}-1) = -T\,\Gamma^{\alpha\alpha,\beta\beta}_{\mathrm{i}\omega_m=0}(\mathrm{i}\nu_l,\mathrm{i}\nu_n), \tag{24}$$

where the right-hand side is the full vertex function of equation (15). The functional Φ must exist because the vertex function is well-defined and the curl of the self-energy vanishes: $\delta\Sigma(\mathrm{i}\nu_n)_{\alpha\alpha}/\delta G(\mathrm{i}\nu_l)_{\beta\beta} - \delta\Sigma(\mathrm{i}\nu_l)_{\beta\beta}/\delta G(\mathrm{i}\nu_n)_{\alpha\alpha} = 0$. So despite the absence of a diagrammatic perturbation theory, the DMFT of the DE model is Φ-derivable and hence, thermodynamically consistent.

4. Transition temperatures

Since the electronic spin-susceptibility is given by $\chi^{\rm el}(\mathbf{q}) = \sum_{l,n} \chi^s_{\mathbf{q},{\rm i}\omega_m=0}({\rm i}\nu_l, {\rm i}\nu_n)$, the condition that $\chi^{\rm el}(\mathbf{q})$ diverges is equivalent to the condition that $\mathrm{Det}(\underline{\chi}^s_{\mathbf{q},{\rm i}\omega_m=0})^{-1} = 0$. To obtain the FM or AF transition temperatures, we require the $\mathbf{q} = 0$ or $\mathbf{Q}$ susceptibilities with $\omega_m = 0$. The AF wavevector $\mathbf{Q}$ is defined so that the Fermi surface is nested at half filling or $\epsilon_{\mathbf{k}+\mathbf{Q}} = -\epsilon_{\mathbf{k}}$. Although the Bethe lattice sketched in figure 1 lacks translational symmetry and nonzero wavevectors $\mathbf{q}$ are ill-defined, the AF wavevector $\mathbf{Q}$ may be associated with the bipartite nature of the Bethe lattice. To be safe, the Néel temperature will be evaluated in two different ways, only one of which relies on the existence of an AF wavevector.

For either FM or AF ordering, the electron filling p can be related to the chemical potential μ through the relation

$$p = 1 + T\sum_n \mathrm{Re}\, G({\rm i}\nu_n) = 1 - \frac{32}{W^2} T \sum_n \mathrm{Re}\, R_n, \tag{25}$$

where $G_0({\rm i}\nu_n)^{-1} = z_n + R_n$ and the complex function R_n satisfies the implicit relation

$$a_n R_n + \frac{W^2}{16}(z_n + R_n) = 0. \tag{26}$$

Since $a_n = (z_n + R_n)^2 - J^2$, R_n falls off like $-W^2/(16 z_n)$ for large n. Notice that $p = 1$ when $\mu = 0$. Since all of our results are particle–hole symmetric about $p = 1$, we shall restrict consideration to the range $0 \leqslant p \leqslant 1$.

As discussed in section 2, the BS equations decouple into charge and spin relations. Since the charge vertex function $\Gamma^c_{{\rm i}\omega_m}({\rm i}\nu_l, {\rm i}\nu_n) = 6B^l_m \delta_{ln}$ is diagonal in Matsubara space, the condition $\mathrm{Det}(\underline{\chi}^c_{\mathbf{q},{\rm i}\omega_m=0})^{-1} = 0$ has no solution for $\mathbf{q} = 0$ or $\mathbf{Q}$. In other words, there is no charge-density wave instability within the DE model.

4.1. FM ordering

When $\mathbf{q} = 0$, the bare zero-frequency lattice susceptibility is given by

$$\chi^{(0)}_{\mathbf{q}=0,{\rm i}\omega_m=0}({\rm i}\nu_l, {\rm i}\nu_n) = \frac{4T}{W^2}\left(1 - \frac{z_l - J^2 G_0({\rm i}\nu_l)}{\sqrt{(z_l - J^2 G_0({\rm i}\nu_l))^2 - W^2/4}}\right)\delta_{ln}. \tag{27}$$

With the help of equation (26), we find that the full spin-susceptibility at $\mathbf{q} = 0$ satisfies

$$\begin{aligned}\chi^{s-1}_{\mathbf{q}=0,{\rm i}\omega_m=0}({\rm i}\nu_l, {\rm i}\nu_n) &= \chi^{(0)-1}_{\mathbf{q}=0,{\rm i}\omega_m=0}({\rm i}\nu_l, {\rm i}\nu_n) - \Gamma^s_{{\rm i}\omega_m=0}({\rm i}\nu_l, {\rm i}\nu_n) \\ &= -2\beta\delta_{ln}\frac{a_l}{(z_l + R_l)b_l}\{(z_l + R_l)^2(z_l + 2R_l) - J^2(z_l + 4R_l/3)\} - \frac{4\beta J^2}{3(1+C)}\frac{a_l a_n}{b_l b_n},\end{aligned} \tag{28}$$

where $b_l = (z_l + R_l)^2 - J^2/3$. Consequently, the condition that $\mathrm{Det}(\underline{\chi}^s_{\mathbf{q}=0,{\rm i}\omega_m=0})^{-1} = 0$ can be written as an implicit condition for the Curie temperature:

$$\frac{2J^2}{3}\sum_n \frac{R_n}{(z_n + R_n)^2(z_n + 2R_n) - J^2(z_n + 4R_n/3)} = 1, \tag{29}$$

which must be supplemented by equation (25) for the electron filling.

If $J/W > 1/4$, the interacting DOS splits into two bands [16]. In the lower band centred at $-J$ with $0 \leqslant p \leqslant 1$, all electrons have their spins parallel to the local moments; in the upper band centred at J with $1 \leqslant p \leqslant 2$, all holes have their spins parallel to the local moments. As J/W increases, both upper and lower bands are narrowed by correlations and their widths approach $W' = W/\sqrt{2}$. To recover the large J limit, the chemical potential must be written as $\mu = J\,\mathrm{sgn}(p-1) + \delta\mu$ where $-W'/2 \leqslant \delta\mu \leqslant W'/2$. Equation (29) then reduces to [14, 15]

$$\sum_n \frac{R_n^2}{R_n^2 - 3W^2/32} = 1, \tag{30}$$

where R_n is now given explicitly by $R_n = (\sqrt{z_n^2 - W^2/8} - z_n)/2$. So in this limit, T_C is proportional to W and is independent of J. Due to the strong Hund's coupling, T_C vanishes at half filling ($p = 1$) or when the lower band is completely full because electrons are unable to hop to neighbouring sites.

In the weak-coupling regime of $T \ll J \ll W$, the summation in equation (29) may be replaced by an integral over frequency ν, as shown in appendix A. Carefully treating the branch cut along the real axis between $\pm W/2$, we find that

$$T_C = \frac{32J^2}{9\pi W}\sqrt{1-(2\mu/W)^2}\{(2\mu/W)^2 - 1/4\}, \tag{31}$$

which is proportional to J^2/W as expected in the RKKY limit. For small filling (μ close to $-W/2$) and a fixed J, T_C initially increases with p and then begins to decrease, vanishing at $\mu = W/4$ corresponding to a filling of $p \approx 0.39$. Because $T_C(p, J)$ is particle-hole symmetric, it is the same for p electrons ($2-p$ holes) and $2-p$ electrons (p holes) per site. These results are in qualitative agreement with Nolting *et al* [28, 29], who evaluated the Curie temperature of the $s-f$ model with quantum local spins using both equations-of-motion [28] and modified RKKY [29] techniques. Nolting *et al* obtained FM solutions for small J in a concentration range significantly narrower than found here, probably because their approach retains the non-local fluctuations produced by the RKKY interaction.

For small fillings and $\varepsilon \equiv 2\mu/W + 1 \ll 1$, $T_C W/J^2 \approx 8\sqrt{2}\varepsilon^{1/2}/(3\pi)$. Since $p \approx 8\sqrt{2}\varepsilon^{3/2}/(3\pi)$, T_C grows like $p^{1/3}$ for small p.

4.2. AF ordering

This section presents two calculations for the AF Néel temperature: one based on the magnetic susceptibility and the other on coupled Green's functions. Their equivalence was established in section 3, which demonstrated that the DMFT of the DE model is thermodynamically consistent. While the first technique explicitly assumes the existence of an AF wavevector $\mathbf{Q}$, the second does not.

4.2.1. From the susceptibility. Evaluating the Néel temperature from the susceptibility requires the bare, zero-frequency lattice susceptibility for $\mathbf{q} = \mathbf{Q}$:

$$\chi^{(0)}_{\mathbf{Q},i\omega_m=0}(i\nu_l, i\nu_n) = -\frac{4T}{W^2}\left(1 - \frac{\sqrt{(z_l - J^2G_0(i\nu_l))^2 - W^2/4}}{z_l - J^2G_0(i\nu_l)}\right)\delta_{ln}. \tag{32}$$

After some algebra, we find that the full spin-susceptibility at $\mathbf{q} = \mathbf{Q}$ satisfies

$$\chi^{s\,-1}_{\mathbf{Q},\mathrm{i}\omega_m=0}(\mathrm{i}\nu_l, \mathrm{i}\nu_n) = \chi^{(0)-1}_{\mathbf{Q},\mathrm{i}\omega_m=0}(\mathrm{i}\nu_l, \mathrm{i}\nu_n) - \Gamma^{s}_{\mathrm{i}\omega_m=0}(\mathrm{i}\nu_l, \mathrm{i}\nu_n)$$
$$= -2\beta\delta_{ln}\frac{a_l}{(z_l + R_l)b_l}\{z_l(z_l + R_l)^2 - J^2(z_l + 2R_l/3)\} - \frac{4\beta J^2}{3(1+C)}\frac{a_l a_n}{b_l b_n}. \tag{33}$$

Consequently, T_N is found from the condition that $\mathrm{Det}(\underline{\chi}^{s}_{\mathbf{Q},\mathrm{i}\omega_m=0})^{-1} = 0$ or

$$-\frac{2J^2}{3}\sum_n \frac{R_n}{z_n(z_n + R_n)^2 - J^2(z_n + 2R_n/3)} = 1, \tag{34}$$

which bares some similarity to equation (29) for T_C.

In the strong-coupling limit, equation (34) reduces to

$$\sum_n \frac{R_n^2}{R_n^2 + 3W^2/32} = 1, \tag{35}$$

with a plus sign multiplying $3W^2/32$ compared to the minus sign in equation (30). It is straightforward to show that $T_\mathrm{N} \leqslant 0$ for all p in this limit. Hence, the AF phase instabilities disappear as $J/W \to \infty$.

In the weak-coupling regime, we may once again replace the Matsubara sum by an integral, with the result

$$T_\mathrm{N} = \frac{8J^2}{3\pi W}\left\{\log\left(\frac{1 + \sqrt{1 - (2\mu/W)^2}}{2|\mu|/W}\right) - \sqrt{1 - (2\mu/W)^2} - \tfrac{4}{3}(1 - (2\mu/W)^2)^{3/2}\right\}. \tag{36}$$

For $p < 0.73$, T_N is negative so the system becomes FM for $0 < p \leqslant 0.39$.

Close to half filling, T_N given by equation (36) becomes positive and the DE model supports an AF phase. We find that $T_\mathrm{N} > 0$ for $0.73 \leqslant p \leqslant 1$, in which range T_C given by equation (31) is negative. The divergence of T_N in equation (36) as $p \to 1$ or $\mu \to 0$ signals a breakdown in the weak-coupling expansion and the appearance of a gap in the interacting DOS, as discussed later.

4.2.2. From coupled Green's functions. The previous subsection used the nesting condition for the AF wavevector $\mathbf{Q}$ whereas, strictly speaking, nonzero wavevectors are not defined on the Bethe lattice. Hence, it is worthwhile to re-evaluate T_N using a Green's function approach that skirts the question of whether an AF wavevector exists. This Green's function approach will also come in handy when considering the SRO state later in section 4.

Dividing the Bethe lattice into A and B sub-lattices, we obtain coupled relations between the bare and full local Green's functions:

$$\underline{G}^{(\eta)}_0(\mathrm{i}\nu_n)^{-1} = z_n\underline{I} - \frac{W^2}{16}\underline{G}^{(\bar{\eta})}(\mathrm{i}\nu_n), \tag{37}$$

where $\eta = \uparrow$ or $\downarrow$ on the A or B sites and $\bar{\eta}$ is opposite to η. If the bare inverse Green's function is parameterized as

$$\underline{G}^{(\eta)}_0(\mathrm{i}\nu_n)^{-1} = (z_n + R_n)\underline{I} + Q^{(\eta)}_n\underline{\sigma}_z, \tag{38}$$

then equation (37) implies that R_n and $Q_n^{(\eta)}$ are solved from the condition

$$R_n \underline{I} + Q_n^{(\eta)} \underline{\sigma}_z = -\frac{W^2}{16} \left\langle \left\{ (z_n + R_n)\underline{I} + \underline{\sigma} \cdot \left(J\mathbf{m} + Q_n^{(\bar{\eta})} \mathbf{z} \right) \right\}^{-1} \right\rangle_{\bar{\eta}}. \tag{39}$$

To linear order in the sublattice magnetization, R_n and $Q_n^{(\eta)}$ satisfy the implicit relations

$$a_n R_n = -\frac{W^2}{16}(z_n + R_n), \tag{40}$$

$$Q_n^{(\eta)} = \frac{R_n}{z_n + R_n} \left\{ Q_n^{(\bar{\eta})} \left(1 + \frac{2J^2}{3a_n} \right) + JM^{(\bar{\eta})} \right\}, \tag{41}$$

where $\langle \mathbf{m} \rangle_\eta \equiv M^{(\eta)} \mathrm{z} = \pm M \mathrm{z}$, the sign depending on whether $\eta = \uparrow$ (A site) or $\eta = \downarrow$ (B site).

The linear relations for $Q_n^{(\eta)}$ may be readily solved, with the result

$$Q_n^{(\eta)} = \frac{M^{(\eta)} J a_n R_n}{(z_n + R_n)^2 z_n - J^2 (z_n + 2R_n/3)}. \tag{42}$$

After integrating $\exp(-S_{\mathrm{eff}}(\mathbf{m}))$ over the Grassman variables, we find that the probability for the local moment on sublattice η to point along $\mathbf{m}$ is

$$P(\mathbf{m})^{(\eta)} \propto \exp\left\{ \sum_n \log\left(1 - \frac{2JQ_n^{(\eta)} m_z}{a_n} \right) \right\} \propto \exp(\beta J_{\mathrm{eff}} M^{(\eta)} m_z). \tag{43}$$

The last relation defines the effective interaction:

$$J_{\mathrm{eff}} = -\frac{2TJ}{M^{(\eta)}} \sum_n \frac{Q_n^{(\eta)}}{a_n} = -2TJ^2 \sum_n \frac{R_n}{z_n (z_n + R_n)^2 - J^2 (z_n + 2R_n/3)}, \tag{44}$$

which is the same on each sublattice. Finally, T_{N} is solved from the condition $M^{(\eta)} = J_{\mathrm{eff}} M^{(\eta)} \beta / 3$, which reproduces equation (34). So the earlier results for T_{N} do not depend on the existence of an AF wavevector.

4.3. Other magnetic phases

Earlier studies of the Heisenberg model on the Bethe lattice [30, 31] proposed a spiral magnetic state with a wavevector that characterizes the twist of the spin between nearest neighbours. But it is quite easy to show that a Bethe lattice cannot be partitioned into more than two sublattices. For example, if we try to partition a Bethe lattice with $z_{\mathrm{c}} = 4$ into three sublattices, then sites C and A (red and purple dots in figure 3(a)) would be next-nearest neighbours but the two sites C (purple dots) (presumably on the same magnetic sublattice) are actually next-nearest neighbours of each other. So unless the central site is singled out, a Bethe lattice does not support a magnetic state with more than two sublattices.

More recently, Gruber *et al* [32] argued that this restriction may be removed as $z_{\mathrm{c}} \to \infty$ because the paths with the largest weight always move outward from the central site. This analysis uses the fact that the surface of the Bethe lattice contains a non-vanishing fraction of its

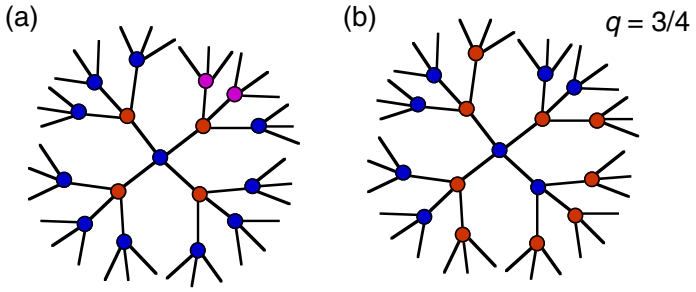

Figure 3. (a) A possible partitioning of the Bethe lattice into three sublattices with blue, red, and purple sites. (b) A colinear SRO state on a $z_c = 4$ Bethe lattice with $q = 3/4$, meaning that $1/4$ of the neighbours of any site have the same spin while $3/4$ have the opposite spin. The two spins are denoted by blue and red dots.

sites [33]. Since the period-three state constructed in [32] can only be formed around a central site, it is not isotropic. Such states will not be considered further in this paper.

The class of SRO states first introduced in an earlier paper [20] is characterized by the correlation parameter $q = \langle \sin^2(\theta_i/2) \rangle$, where the average is taken over all neighbours of any site on the Bethe lattice. Since the azimuthal angles ϕ_i of the neighbouring spins are assumed to be random with $\langle \exp(\mathrm{i}\phi_i) \rangle = 0$, the neighbouring spins will on average sweep out a cone with angle $2 \arcsin(\sqrt{q})$ about the central spin. Due to the topology of the Bethe lattice, an SRO phase cannot be ordered (except in the FM or AF limits when $q = 0$ or 1). For the special case of a colinear SRO state, $\theta_i = 0$ or π on every site and q is the fraction of neighbours of any site that have the opposite spin. An example of a colinear SRO state with $z_c = 4$ and $q = 3/4$ is sketched in figure 3(b).

Quite generally, the SRO phase has short-range but not long-range magnetic order. If M_n is the average magnetization of the lattice sites at a distance na (lattice constant a) from a central site, then it is easy to show that $M_n = (1 - 2q)M_{n-1}$. So the magnetization decays exponentially like $|M_n| = |M_0| \exp(-na/\xi)$ with the correlation length $\xi = -a/\log|2q - 1| \geqslant 0$. The correlation length diverges in the FM and AF limits and vanishes in the NM state with $q = 1/2$, when the spins around any site are completely disordered. An SRO phase can have either FM ($0 < q < 1/2$) or AF ($1/2 < q < 1$) correlations, as discussed further below.

Also working on the Bethe lattice, Chattopadhyay *et al* [5] assumed that all of the angles θ_i were identical and characterized the resulting state by its 'incommensurate spin correlations.' We avoid this description because nonzero wavevectors are ill-defined on the Bethe lattice and the $X(\mathbf{q})$ formalism of Müller-Hartmann [8] cannot be adapted from the hypercubic to the Bethe lattice. In our view, the SRO phase is more accurately characterized by the magnetic correlations around any site.

In the absence of the SRO states, a large portion of the magnetic phase diagram is NM. This poses a problem because Nernst's theorem requires that the entropy vanishes at $T = 0$. Generally, the entropy of an SRO state is difficult to evaluate. But in the $z_c \to \infty$ limit, the entropy of a collinear SRO phase is

$$\frac{S_{\mathrm{col}}}{N} = -q \log q - (1 - q) \log(1 - q), \tag{45}$$

which vanishes only in the FM or AF phases. Of course, the entropy of a non-collinear SRO phase must be greater than $S_{\rm col}$. Therefore, the formal dilemma posed by Nernst's theorem is not resolved by the presence of SRO states. As discussed in the conclusion, entropic ground states frequently arise in infinite dimensions. In finite dimensions, the SRO state may evolve into a state with incommensurate SRO.

Since an SRO phase with correlation parameter q between 0 and 1 has no long-range order, the transition temperature $T_{\rm SRO}(p,q)$ cannot be obtained from the condition that the magnetic susceptibility diverges. But we can easily solve for $T_{\rm SRO}(p,q)$ by generalizing the Green's function technique used in subsection 4.2.2. With the SRO state defined above, the self-consistency relation between the bare and full local Green's functions is derived in appendix B:

$$\underline{G}_0^{(\eta)}(\mathrm{i}\nu_n)^{-1} = z_n \underline{I} - \frac{W^2}{16}\left\{q\underline{G}^{(\bar{\eta})}(\mathrm{i}\nu_n) + (1-q)\underline{G}^{(\eta)}(\mathrm{i}\nu_n)\right\}, \tag{46}$$

where $\underline{G}^{(\eta)}$ and $\underline{G}^{(\bar{\eta})}$ are spin-reversed Green's functions. The quantization axis η is defined by the spin on the central site 0. The above relation was previously obtained in [5] under the more restrictive condition that θ_i is constant. Once again parameterizing the bare inverse Green's function by equation (38), we find that R_n is independent of the magnetization $M = \langle m_z \rangle$ on site 0 (assumed spin up) and is given by equation (40) while $Q_n^{(\uparrow)} = -Q_n^{(\downarrow)}$ has the linearized solution

$$Q_n^{(\uparrow)} = \frac{(2q-1)MJa_nR_n}{(z_n+R_n)^2(z_n+2(1-q)R_n) - J^2(z_n+2(2-q)R_n/3)}, \tag{47}$$

which reduces to equation (42) when $q = 1$.

The effective interaction $J_{\rm eff}$ is again given by the first equality in equation (44) so that $T_{\rm SRO}(p,q)$ is solved from the implicit relation

$$-\frac{2J^2}{3}(2q-1)\sum_n \frac{R_n}{(z_n+2(1-q)R_n)(z_n+R_n)^2 - J^2(z_n+2(2-q)R_n/3)} = 1, \tag{48}$$

which reduces to both the FM and AF results, equations (29) and (34), when $q = 0$ and $q = 1$. It also follows that $T_{\rm SRO}(p,q) = 0$ in the NM state with $q = 1/2$.

In the strong-coupling limit $W \ll J$ and $T \ll J$, $T_{\rm SRO}(p,q)$ is solved from the condition

$$\sum_n \frac{R_n^2}{R_n^2 + 3W^2/(32(2q-1))} = 1. \tag{49}$$

It is straightforward to show that $T_{\rm SRO}(p,q)$ is negative for $1/2 \leqslant q \leqslant 1$ and is positive but always smaller than $T_{\rm C}(p)$ for $0 \leqslant q < 1/2$. So as expected, the SRO states are unstable in the strong-coupling limit.

Results for $T_{\rm SRO}(p,q)$ in the weak-coupling limit are given in appendix A. Maximizing $T_{\rm SRO}(p,q)$ with respect to q, we obtain $T_{\rm SRO}^{(\max)}(p)$ plotted in figure 4. Remarkably, an SRO phase with AF correlations can always be found with a higher transition temperature than the AF state. As $q \to 1$, the AF and SRO transition temperatures meet at $p = 1$ or half filling. Even in the range of fillings between about 0.26 and 0.39, where $T_{\rm C}$ is nonzero, an SRO phase with

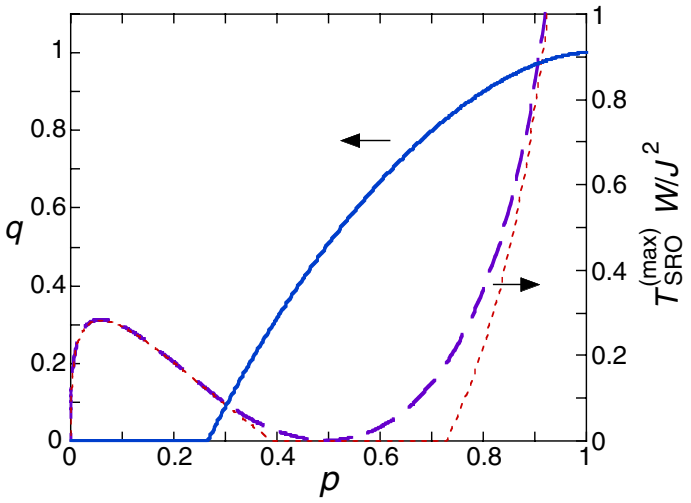

Figure 4. The correlation parameter q (solid line) and the associated maximum SRO transition temperature $T_{\mathrm{SRO}}^{(\max)}(p)$ (dashed line) versus filling p for the SRO states in the weak-coupling limit. Also plotted in the thin short-dashed line are the weak-coupling limits of T_{C} for $q = 0$ and T_{N} for $q = 1$.

FM correlations or $0 < q < 1/2$ has the higher critical temperature. Also notice that the SRO transition temperature is nonzero in the range of fillings between 0.39 and 0.73, where neither the FM nor AF states was stable for small J/W. The point at which $q = 1/2$ and $T_{\mathrm{SRO}}^{(\max)}(p) = 0$ lies slightly below $p = 0.5$. Recall that q changes discontinuously at $T_{\mathrm{SRO}}^{(\max)}(p)$ from $1/2$ in the NM phase above to a value greater than or smaller than $1/2$ in the SRO phase below.

5. Magnetic instabilities of the DE model

We shall first present results for the magnetic transition temperatures in the absence of the SRO states. These results are then revised to include the SRO states. Bear in mind that just because a FM, AF, or SRO state has the highest transition temperature for a given J/W and p does not imply that it remains stable down to zero temperature or even that it is reached at all: a pure state may be bypassed by the formation of a PS mixture. The issue of PS can only be resolved by calculating the free energy as a function of filling. We shall perform such a study for $T = 0$ in section 4.

In figure 5, the Curie and Néel temperatures are plotted versus filling for a variety of couplings. When $p \geqslant 0.39$, a critical value of J is required for T_{C} to be nonzero. So the weak-coupling regime is restricted to electron concentrations smaller than 0.39. As J/W increases, the AF instabilities are restricted to a narrower range of concentrations near $p = 1$. For large J/W at half filling, the nearest-neighbour hopping can be treated perturbatively and superexchange leads to a Néel temperature proportional to W^2/J. So the sliver of AF phase stabilized around half filling rapidly narrows with increasing J/W. By contrast the FM phase dominates as J/W increases. In the limit $J/W \to \infty$, the Néel temperature vanishes even at $p = 1$.

For a fixed filling, T_{C} and T_{N} are plotted versus J/W in figure 6. As expected, the weak-coupling curves track the numeric results for small J/W but deviate for larger J/W. Whereas the

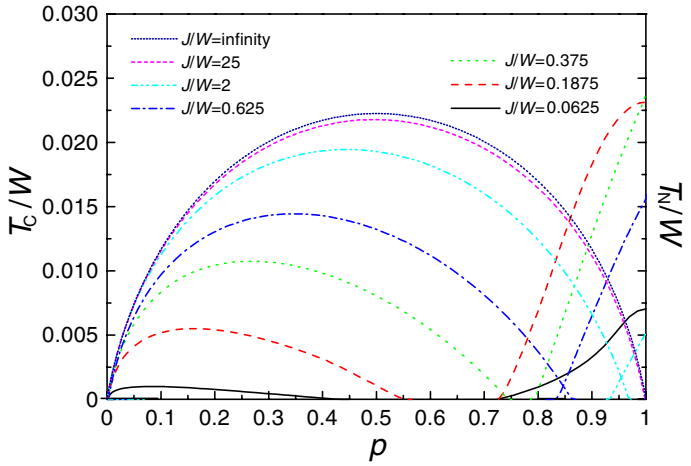

Figure 5. The Curie and Néel temperatures versus filling p for a variety of couplings J/W.

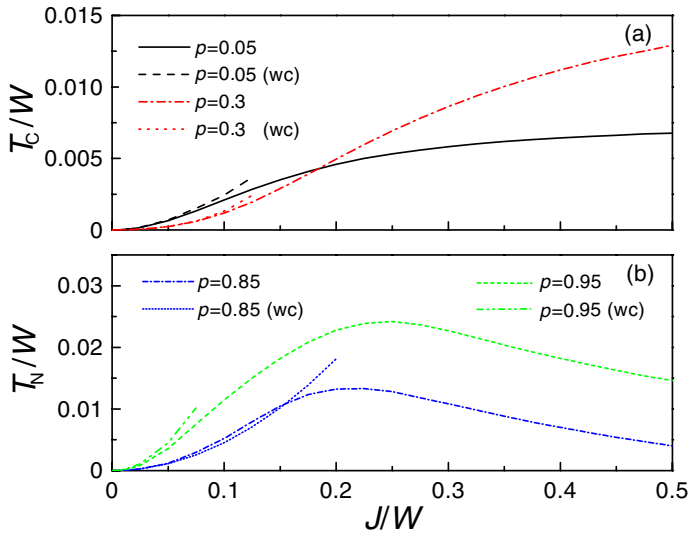

Figure 6. The (a) Curie and (b) Néel temperatures versus J/W for several fillings. Also shown are the weak-coupling transition temperatures obtained using perturbation theory.

Curie temperature reaches a plateau at a value of order W, the Néel temperature for any $p < 1$ vanishes at a finite value of J/W. Again, the filling range of AF instabilities rapidly narrows as J/W increases.

The phase instabilities of the DE model in the absence of SRO states are plotted in figure 7(a). The NM region shrinks as J/W increases and is absent for $J/W > 0.5$. Since the interacting DOS splits for $J/W > 1/4$ [16], the NM region survives even after the formation of sub-bands. Whereas the AF region persists at half filling for all J/W, the sliver of AF phase rapidly narrows with increasing coupling. The FM/NM phase boundary in figure 7(a) agrees quite well with that found by Auslender and Kogan [14].

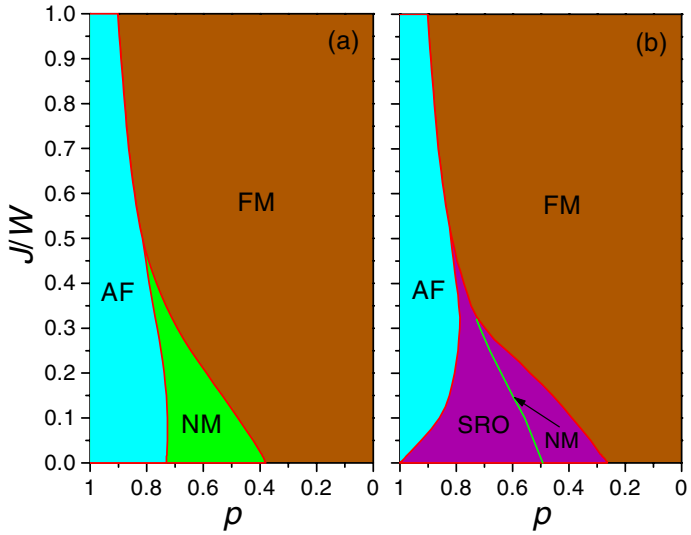

Figure 7. The phase instabilities of the DE model (a) assuming only FM, AF and NM phases and (b) also including the SRO phase.

Now including the SRO states, we plot the correlation parameter q along with $T_{\mathrm{SRO}}^{(\max)}(p)$ in figure 8. For $J/W > 0$, a transition into the AF state ($q = 1$) occurs in a narrow range of fillings close to $p = 1$. This range vanishes both as $J/W \to 0$ and as $J/W \to \infty$. It has a maximal extent (from $p = 0.78$ to 1) when $J/W \approx 0.33$. For $J/W < 0.33$, $T_{\mathrm{SRO}}^{(\max)}(p)$ vanishes at a single filling that corresponds to $q = 0.5$, meaning that there is no SRO. For $0.5 > J/W > 0.33$, $T_{\mathrm{SRO}}^{(\max)}(p)$ is nonzero for all fillings. As can be seen in figure 8(a) for $J/W = 0.375$, the correlation parameter for $0.5 > J/W > 0.33$ jumps from $q = 0$ in the FM phase to a nonzero value $0.5 < q < 1$ in the SRO phase. For $J/W > 0.5$, one of the ordered phases always has a higher transition temperatures than the SRO states and q jumps from 0 to 1 at the FM/AF boundary. The deviation between the numeric and weak-coupling results in figure 8(c) as $p \to 1$ is quite expected: in the limit $p \to 1$, the weak-coupling result for the SRO transition temperature diverges, thereby invalidating the condition $T \ll J$ under which it was derived.

The magnetic instabilities of the DE model including SRO states are mapped in figure 7(b). Notice that the region formerly labelled NM in figure 7(a) is now occupied by SRO states. The SRO phase also occupies the formerly AF region at very small J/W. As anticipated above, the NM curve (where $T_{\mathrm{SRO}}^{(\max)}(p) = 0$ and $q = 1/2$) intersects the FM phase boundary at $J/W \approx 0.33$. This curve separates an SRO region with AF correlations ($1 > q > 1/2$) on the left from an SRO region with FM correlations ($1/2 > q > 0$) on the right.

6. Magnetic phase diagram of the DE model

The presence of a continuous range of SRO states with correlation parameter q obviously complicates the magnetic phase diagram of the DE model and the issue of PS. Because the weak-coupling behaviour of the DE model has been the subject of some debate [3]–[5], [14], we shall treat this limit analytically. We then provide numerical results for the interacting DOS that

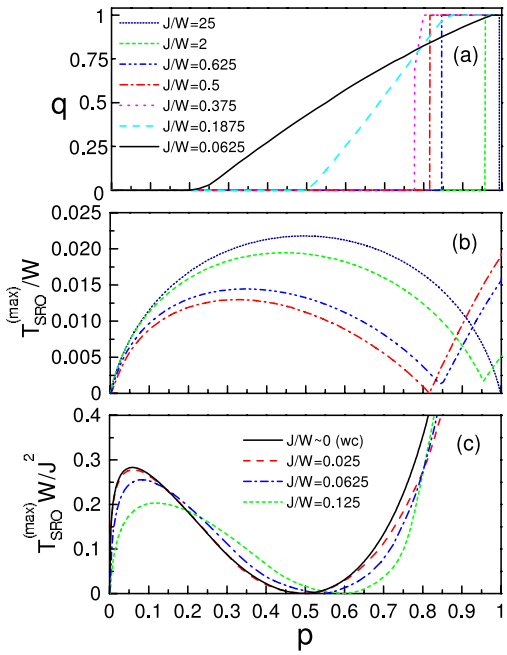

Figure 8. (a) The correlation parameter q, (b) the maximum transition temperature $T_{\mathrm{SRO}}^{(\max)}(p)/W$, and (c) the normalized transition temperature $T_{\mathrm{SRO}}^{(\max)}(p)W/J^2$ for various values of J/W versus filling p.

explain the stability of the SRO phase. Finally, we present the $T = 0$ phase diagram of the DE model, both with and without the SRO states.

6.1. Weak-coupling limit

In their numerical work at $T = 0$, Chattopadhyay *et al* [5] obtained a very complex phase diagram, with a range of SRO states above $J/W \approx 1/16$ and PS between AF and FM phases for $0.1 < p < 1$ below this value. For small J/W, a pure FM phase was found to be stable for $0 < p \leqslant 0.1$. We now show that PS disappears in the exactly solvable limit of zero temperature and weak coupling.

At zero temperature, the FM, AF, and SRO energies are evaluated after once again parameterizing $\underline{G}_0^{(\eta)}(z = \mathrm{i}\nu + \mu)^{-1}$ by equation (38). Then, $R(z)$ is obtained from the quartic equation

$$R(z+R)\{(z+2(1-q)R)^2 - J^2\} + \frac{W^2}{16}(z+2(1-q)R)^2 = 0, \tag{50}$$

which differs from equation (26) (except when $q = 1/2$) because we are now working in the broken-symmetry phase. Similarly, $Q^{(\uparrow)}(z) = -Q^{(\downarrow)}(z)$ is given by

$$Q^{(\uparrow)}(z) = (2q-1)\frac{MJR(z)}{z+2(1-q)R(z)}, \tag{51}$$

which is likewise valid for any J.

The potential energy can generally be written as $\langle V\rangle/N = -2JM\langle s_{0z}\rangle$, where the expectation value of the electronic spin on site 0 for any temperature is

$$\langle s_{0z}\rangle = \frac{1}{4\pi}\int \mathrm{d}\nu\, \mathrm{Re}\, G^{(\uparrow)}(z)_{\alpha\beta}\sigma^{z}_{\beta\alpha} = \frac{8}{\pi W^2(2q-1)}\int \mathrm{d}\nu\, Q^{(\uparrow)}(z). \tag{52}$$

For any J, the potential energy may be written as

$$\frac{1}{N}\langle V(p,q)\rangle = -\frac{16J^2}{\pi W^2}\int \mathrm{d}\nu \frac{R(z)}{z+2(1-q)R(z)}. \tag{53}$$

Of course, the NM potential energy is obtained by setting $q = 1/2$.

Second-order results for $\langle V(p,q)\rangle/N$ are provided in appendix A. For small J/W, $\langle s_{0z}\rangle$ is of order J/W so the electronic spins are not frozen at $T = 0$. Bearing in mind that $T_{\mathrm{SRO}}(p, q = 0) = T_{\mathrm{C}}(p)$ and $T_{\mathrm{SRO}}(p, q = 1) = T_{\mathrm{N}}(p)$, the difference between the potential energies of a FM, AF, or SRO phase and a NM is given by $\Delta\langle V(p,q)\rangle/N = -3T_{\mathrm{SRO}}(p,q)$, where both sides are evaluated to order J^2/W. So the potential energy is lowered when the transition temperature is positive.

A general expression for the kinetic energy of the SRO phase is proven in appendix C. At $T = 0$, equation (C.3) becomes

$$\frac{1}{N}\langle K\rangle = \frac{W^2}{64\pi}\sum_{\eta}\int \mathrm{d}\nu\, G^{(\eta)}(z)_{\alpha\beta}\{(1-q)G^{(\eta)}(z)_{\beta\alpha} + qG^{(\bar{\eta})}(z)_{\beta\alpha}\}. \tag{54}$$

In contrast to alternative expressions for the kinetic energy of the FM and AF phases [10], equation (54) does not assume any particular wavevector for the ground state. Independent of q, the zeroth-order kinetic energy is given by $E_0(p)/N = -2W/(3\pi)(1-\delta^2)^{3/2}$, where $\delta = 2\mu_0/W$ and μ_0 is the chemical potential evaluated to zeroth-order in J/W. For any J, the SRO kinetic energy is given by

$$\frac{1}{N}\langle K(p,q)\rangle = \frac{16}{\pi W^2}\int \mathrm{d}\nu\, R(z)^2\left\{1 + \frac{(1-2q)J^2}{(z+2(1-q)R(z))^2}\right\} \tag{55}$$

and the NM kinetic is recovered by setting $q = 1/2$. It is important to realize that the second-order kinetic energy contains two contributions: one from the dependence of the integrand on J/W for a fixed μ; the other from the dependence of the chemical potential $\mu(p)$ on J/W for a fixed p.

Using the condition that $p = 1 - 32/(\pi W^2)\int \mathrm{d}\nu\, \mathrm{Re}\, R(z)$ depends only on the filling and not on J, we may expand μ in powers of J/W as $\mu = \mu_0 + (J/W)^2\mu_2 + \cdots$. Then $\mu_0(p)$ is solved from the condition

$$p = 1 + \frac{2}{\pi}\left\{\delta\sqrt{1-\delta^2} + \sin^{-1}\delta\right\} \tag{56}$$

and $\mu_2(p)$ is given in terms of $\mu_0(p)$ by $\mu_2 = W\delta/\{(1-q)^2 + \delta^2(2q-1)\}$. The divergence of μ_2 as $q \to 1$ and $p \to 1$ (or $\delta \to 0$) signals the opening of a gap in the interacting, AF DOS as discussed further below.

Incorporating the change in chemical potential, the result for the second-order, q-dependent correction to $\langle K(p,q)\rangle/N$ is given in appendix A. To second order in J/W, the difference between the kinetic energies of a FM, AF, or SRO phase and a NM is $\Delta\langle K(p,q)\rangle/N = 3T_{\rm SRO}(p,q)/2$. Hence, kinetic energy is lost (the electrons become more confined) when the transition temperature is positive.

Consequently, the net change in energy $E(p,q) = \langle K(p,q) + V(p,q)\rangle$ in the weak-coupling limit is given by $\Delta E(p,q)/N = -3T_{\rm SRO}(p,q)/2$, which includes the FM ($q = 0$) and AF ($q = 1$) phases as special cases. The same relation would be obtained for a Heisenberg model $H = -(1/2)\sum_{i,j} J_{ij}\mathbf{S}_i \cdot \mathbf{S}_j$ with classical spins within Weiss mean-field theory (which becomes exact in infinite dimensions), so that $\Delta E/N = -J(\mathbf{k} = 0)S^2/2 = -3T_{\rm C}/2$. For large J/W, however, the DE value of $\Delta E(p, q = 0)/N$ in the FM phase is proportional to J whereas $T_{\rm C}$ is proportional to W. So the proportionality between $\Delta E(p,q)/N$ and $T_{\rm SRO}(p,q)$ (and the analogy with the Heisenberg model) only holds in the weak-coupling limit.

In the limit of small J/W, the ground state energy is minimized by the same correlation parameter q that maximizes the transition temperature! This result is not surprising: for small J/W, the transition temperature is also small so the correlation parameter that appears at $T_{\rm SRO}(p,q)$ continues to minimize the energy at $T = 0$. As a consistency check, the results in appendix A may be used to show that the derivative of the energy is related to the chemical potential by $\mathrm{d}E(p,q)/\mathrm{d}p = N\mu$, where both sides are expanded to second order in J/W.

6.2. *Interacting DOS*

To better interpret the weak-coupling results, we construct the interacting DOS per spin

$$N(\omega, q) = -\frac{1}{4\pi}\sum_{\eta} \mathrm{Im}G^{(\eta)}(z \to \omega + \mathrm{i}\delta)_{\alpha\alpha} = \frac{16}{\pi W^2}\mathrm{Im}\{R\}_{z\to\omega+\mathrm{i}\delta}. \tag{57}$$

As $J/W \to 0$, $N(\omega, q)$ reduces to the bare DOS $N_0(\omega)$ for any q. The AF DOS can be solved analytically for all J:

$$N(\omega, q = 1) = \frac{8|\omega|}{\pi W^2}\mathrm{Re}\sqrt{\frac{W^2/4 + J^2 - \omega^2}{\omega^2 - J^2}} \tag{58}$$

which vanishes for $|\omega| < J$ and $|\omega| > \sqrt{W^2/4 + J^2}$. Hence, $N(\omega, q = 1)$ contains a square-root singularity on either side of a gap with magnitude $2J$. As $J/W \to \infty$, the width of each sideband narrows like $W^2/8J$. It is also possible to explicitly evaluate the DOS at $\omega = 0$ for any q: $N(\omega = 0, q) = (8/\pi W^2(1-q))\mathrm{Re}\sqrt{J_{\rm c}^2 - J^2}$, which vanishes for $J > J_{\rm c} \equiv W(1-q)/2$. For a NM, the critical value of J required to split the DOS is $J_{\rm c} = W/4$, as found earlier [16]. For an AF at $T = 0$, $J_{\rm c} = 0$ since a gap forms for any nonzero coupling constant. For an SRO phase, $J_{\rm c} > 0$.

Taking $J/W = 0.2$, we numerically solve for $R(z)$ and plot the interacting DOS versus ω for $q = 0, 1/4, 1/2, 3/4$ and 1 in figure 9. The FM DOS has kinks at $\omega = \pm(W/2 - J)$. For energies between the kinks, both up- and down-spin states appear; on either side of the kinks, the bands are fully spin-polarized. These kinks disappear in an SRO state with $q > 0$ due to the absence of long-range magnetic order. The width of the DOS shrinks as q increases from 0 to 1. These results agree with the second-order change to the chemical potential given above. In fact,

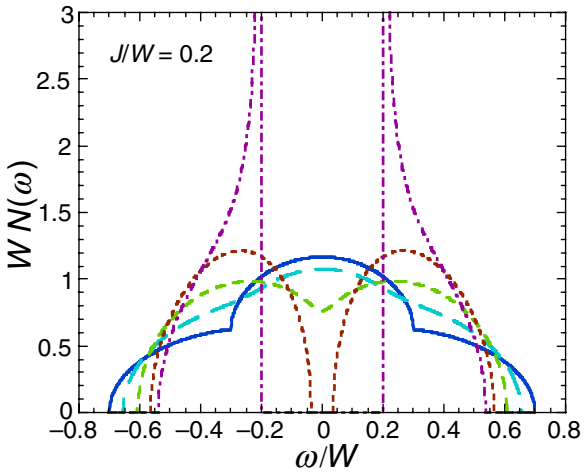

Figure 9. The interacting DOS $N(\omega, q)$ (normalized by $1/W$) versus ω/W for $J/W = 0.2$ in the FM or $q = 0$ (solid, blue), SRO phase with $q = 1/4$ (long dash, light blue), NM or $q = 1/2$ (dash, green), SRO phase with $q = 3/4$ (small dash, red) and AF or $q = 1$ (dot dash, purple) phases.

the divergence of the AF result for μ_2 as $p \to 1$ is caused by the appearance of a gap in the AF DOS for any nonzero J.

For any temperature, coupling constant, and correlation parameter, the total energy of the DE model may be written as an integral over the interacting DOS:

$$\frac{1}{N}E(p, q) = 2\int \mathrm{d}\omega\, \omega f(\omega) N(\omega, q), \tag{59}$$

where $f(\omega) = 1/(\exp(\beta(\omega - \mu)) + 1)$ is the Fermi function and $\mu = \mu(p)$. At $T = 0$, this relation may be expressed in the compact form

$$\frac{1}{N}E(p, q) = -\frac{1}{\pi}\int \mathrm{d}\nu \left\{1 + \frac{16 z R(z)}{W^2}\right\}, \tag{60}$$

which agrees with equations (53) and (55).

From these results, it is not hard to understand why an SRO phase can have a lower energy than an AF. Due to the narrowing of the AF DOS, the AF energy may be higher than that of an SRO state with $J < J_c(q)$ and no energy gap. If the chemical potential of the AF phase lies sufficiently far from the energy gap, then the broader DOS of an SRO phase with $J < J_c$ will favour that state over an AF. As $p \to 1$, this condition is impossible to satisfy for arbitrarily small J and the AF becomes stable.

For a given $p < 1$, the expansions of the kinetic and potential energies in powers of $(J/W)^2$ are valid when $J < J_c(q)$ so that the DOS of an SRO state with correlation parameter q is not gapped. Conversely, for a fixed J, the expansions fail sufficiently close to $p = 1$ and $q = 1$ that a gap develops in $N(\omega, q)$.

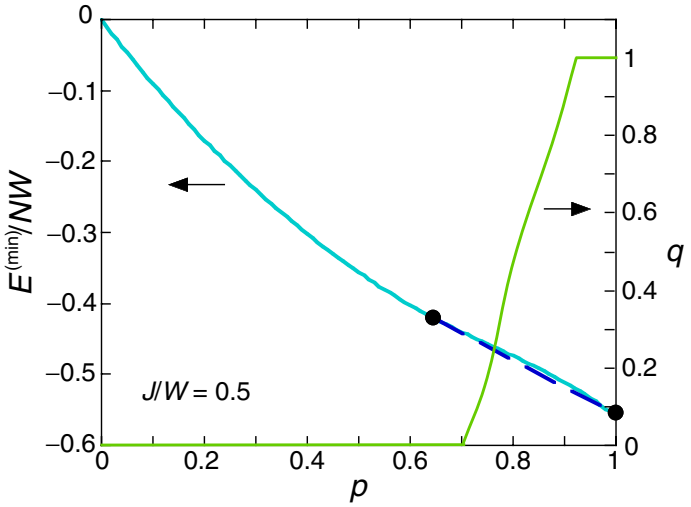

Figure 10. The $T = 0$ energy $E^{(\min)}(p)$ and the value of q that minimizes the energy versus filling for $J/W = 0.5$. A Maxwell constructions (given by the dots and dashed line) between filling $p_1 = 0.647$ and $p_2 = 1$ demonstrates the existence of PS.

6.3. Ground-state phase diagram and PS

When only FM, AF and NM states are considered, PS occurs due to the discontinuity in the chemical potential at the FM/NM and NM/AF phase boundaries. Since these discontinuities become weaker as J/W decreases, PS disappears as $J/W \to 0$.

Once the SRO states are introduced, the physical energy $E^{(\min)}(p)$ is obtained by minimizing $E(p, q)$ with respect to q for a fixed p. Although the chemical potential is a continuous function of filling, PS still occurs for non-zero J due to the formation of an energy gap in the AF state, so that $(1/N)\,\mathrm{d}E^{(\min)}/\mathrm{d}p|_{p=1^-} = -J$. A necessary condition for PS between fillings $p_1 < 1$ and $p_2 = 1$ is that the second derivative of the energy $E^{(\min)}(p)$ must change sign for some filling $p^\star$ between p_1 and p_2. But if $E^{(\min)}(p)$ is expanded in powers of $(J/W)^2$, then the condition that $\mathrm{d}^2E^{(\min)}(p)/\mathrm{d}p^2|_{p^\star} = 0$ may be written

$$\frac{\pi}{8\sqrt{1-\delta^2}} \sim \left.\frac{J^2}{W^2\delta^2}\right|_{p^\star}, \tag{61}$$

where $\delta = 2\mu_0/W$ and μ_0 is the chemical potential evaluated to zeroth-order in J/W. Since the value $q^\star$ of q at $p^\star$ is less than 1, the expansion in powers of $(J/W)^2$ is valid for $J < J_c(q^\star)$, as discussed previously. When $J/W \to 0$, the right-hand side of equation (61) vanishes so the condition for PS cannot be met in the limit of vanishing J/W except as $\delta \to 0$ or $p^\star \to 1$. Near $p = 1$, $\delta \approx (1-p)\pi/4$ so equation (61) also implies that the difference $p_2 - p_1$ grows linearly with J/W. These results contradict Chattopadhyay *et al* [5], who seem to use a Maxwell construction involving the difference $E^{(\min)}(p) - E_0(p)$ rather than the total minimum energy $E^{(\min)}(p)$.

To show this more explicitly, we have used $E^{(\min)}(p)$ to find the PS region through Maxwell constructions between fillings $p_1 < 1$ and $p_2 = 1$. One such Maxwell construction is pictured in figure 10, where a phase mixture along the dashed line provides a lower energy than the pure

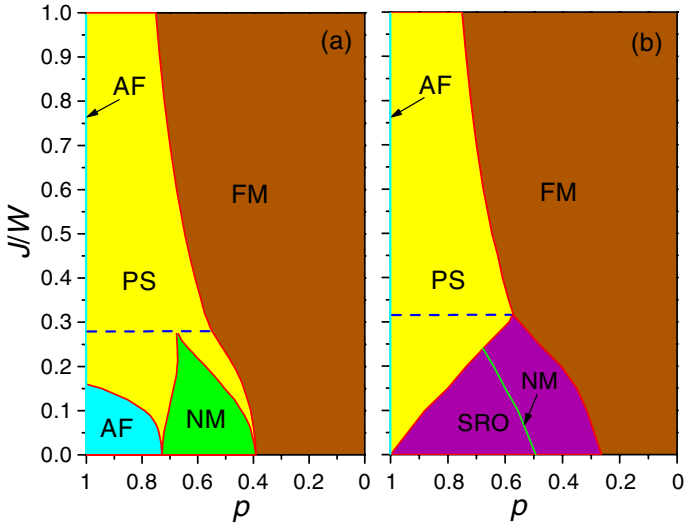

Figure 11. The $T = 0$ magnetic phase diagram of the DE model (a) assuming only FM, AF and NM phases and (b) also including the SRO phase.

phase on the solid curve. For $J/W = 0.5$, the SRO states are bypassed and PS occurs between a FM with $p_1 = 0.647$ and an AF with $p_2 = 1$.

The $T = 0$ phase diagram of figure 11(a) assumes that only the NM, FM and AF phases are allowed. Without the SRO state, the ground-state phase diagram is fairly complicated. As implied by the argument above, PS disappears in the limit of vanishing J/W but the PS regions grow with increasing J/W. Two PS regions appear around the fillings of the AF/NM and NM/FM phase boundaries for $J/W \ll 1$. When $0 < J/W \leqslant 0.16$, the lower PS region in figure 11(a) mixes an AF with $p < 1$ and a NM. For $0.16 < J/W < 0.28$, an AF with $p < 1$ is unstable and the lower PS region mixes an AF with $p = 1$ and a NM. For $J/W > 0.28$, PS occurs between a FM and an AF with $p = 1$.

Surprisingly, the $T = 0$ phase diagram of figure 11(b) becomes much simpler once the SRO states are included. For $J/W < 0.33$, a SRO state is stable over a range of fillings that diminishes with increasing J. Near half-filling, PS is found between an SRO state with $0 < q < 1$ and an AF with $p = 1$. In agreement with the above discussion, the PS region grows linearly with J/W. For $J/W > 0.33$, the SRO phase is skipped and PS occurs between a FM with $q = 0$ and an AF with $p = 1$. The special value $J/W \approx 0.33$ agrees with the coupling where the NM line intersects the FM boundary in the instability map of figure 7(b). It also corresponds to the coupling where the AF instability covers the widest range of fillings.

The PS regions in figures 11(a) and (b) shrink with increasing J/W. In the strong-coupling regime, our results are in qualitative agreement with other authors [3, 11]. But for $J/W = 2$, we obtain PS over a somewhat larger range of fillings than obtained in [13]. Aside from the behaviour at very small J/W, the phase diagram of figure 11(b) agrees rather well with that presented by Chattopadhyay *et al* [5]. In particular, those authors also found that the SRO phase disappears when J/W exceeds about 0.3.

Together, figures 7 and 11 provide a bird's eye view of the magnetic instabilities and phase evolution in the DE model. In figures 7(a) and 11(a), a triangle of phase space remains NM for all temperatures down to $T = 0$; in figures 7(b) and 11(b), a somewhat larger triangle of phase

space remains in the SRO phase down to $T = 0$. Keep in mind, however, that the ordered phases of figure 7 may be bypassed when $\{J/W, p\}$ lies in the PS region of figure 11. For example, Furukawa [13] found that for $J/W = 2$, an AF with $p < 1$ was excluded by PS between an AF with $p = 1$ and a NM.

7. Conclusions

We have used DMFT to evaluate the magnetic phase instabilities and ground-state phase diagram of the DE model. Surprisingly, an SRO phase may have a higher transition temperature than the long-range ordered AF and FM phases. The ground-state phase diagram of the DE model actually simplifies in the presence of the SRO states.

At first sight, the stability of disordered NM and SRO ground states may be hard to understand. After all, the presence of a disordered state at $T = 0$ contradicts Nernst's theorem, which requires that the entropy of the local moments be quenched at zero temperature. However, entropic ground states appear quite frequently in infinite-dimensional calculations. Within the DMFT of the Hubbard model, AF ordering on a hypercubic lattice at half filling can be frustrated by hopping between sites on the same sub-lattice [10]. This additional hopping produces a NM Mott insulator at $T = 0$ for large U/W, again in violation of Nernst's theorem. Also on the hypercubic lattice, the DE model has a NM ground state extending all the way to $p = 0$ when J/W is sufficiently small [4]. Although they did not study such states in detail, Nagai *et al* [4] detected the signature of incommensurate states for weak coupling. Therefore, many-body theories in infinite dimensions are frequently unable to lower the symmetries of disordered ground states. Of course, DMFT cannot access phases described by a non-local order parameter. It should also be noted that Nernst's theorem only applies rigorously to quantum systems and not to a DE model with classical local spins.

For small J/W, the energy of the entropic SRO state is lowered below the energies of the FM and AF phases by the RKKY interaction [7], which generates competing FM and AF interactions [14]. As the dimension is lowered, the SRO state may evolve into the state with incommensurate correlations (IC) obtained in one- and two-dimensional Monte Carlo simulations by Yunoki *et al* [3]. Replacing 'SRO' by 'IC', the phase diagram of figure 11(b) bears a striking resemblance to the phase diagrams of [3]. In agreement with our results, Yunoki *et al* found that the short-range correlations in the IC phase change from AF to FM as p decreases. The phase diagram of figure 11(b) also looks quite similar to the three-dimensional phase diagram obtained by Yin [6], who compared the energies of the AF and FM phases with the energy of a two-dimensional spiral phase carrying momenta along the (111) direction. Hence, the infinite-dimensional phase diagram of figure 11(b) is closely related to the results of finite-dimensional calculations.

On a translationally invariant hypercubic lattice [10] in infinite dimensions, the SRO phase may map onto an incommensurate spin-density wave (SDW) with a definite wavevector. In that case, the transition temperature of the SDW could be obtained from either the coupled Green's functions or the magnetic susceptibility. However, there are no indications for SDW ordering in the limited studies of the DE model on an infinite-dimensional hypercubic lattice [4] and we consider such a possibility to be remote. Much more likely, the SRO phase would map onto a disordered state with short-range magnetic order and broad maxima at wavevectors $\mathbf{q}$ associated with the nesting of the Fermi surface, as found in Monte Carlo simulations of one- and two-dimensional hypercubic lattices [3].

Bear in mind that DMFT studies of the DE model on a hypercubic lattice sacrifice a key advantage of the Bethe lattice: the possibility of obtaining analytic results due to the relationship, equation (6), between the bare and full Green's function. For example, both sides of the expression $\Delta E(p, q)/N = -3T_{\mathrm{SRO}}(p, q)/2$ were evaluated independently to order J^2/W. This gives us great confidence in our results for the energy and critical temperature in the weak-coupling limit. Such analytic results are not possible on a hypercubic lattice. Indeed, pathological results have been found [16] on a hypercubic lattice due to the asymptotic freedom of the quasiparticles in the tails of the Gaussian DOS. In most instances, more physical results are obtained on a Bethe lattice, where the bounded DOS more closely resembles the DOS in two and three dimensions.

Working on a Bethe lattice has allowed us to clarify the behaviour of the DE model at weak coupling. We have demonstrated both analytically and numerically that PS disappears as $J/W \to 0$. Whereas the FM phase is stable for p below about 0.26, an SRO state is stable above. As $p \to 1$, the SRO phase evolves into the long-range ordered AF phase. The transition temperature of the SRO phase exceeds that of the FM and AF phases for $0.26 < p < 1$.

Whether the SRO phase is a new kind of spin glass or a spin liquid can only be resolved by future studies of the static and dynamic susceptibilities. An intriguing possibility is that the local moments are frozen within a spin-glass state but that the electronic spins are subject to quantum fluctuations within a spin-liquid state. Two of the most important unresolved questions about spin glasses are whether there exists a true thermodynamic spin-glass transition [34] and whether a model without quenched disorder can support a spin glass [35]. We have answered those questions for the DE model on an infinite-dimensional Bethe lattice. Above $T_{\mathrm{SRO}}(p, q)$, the NM state is characterized by the absence of SRO around any site. Below $T_{\mathrm{SRO}}(p, q)$, short-range magnetic order develops with a correlation length $\xi(q) = -a/\log|2q - 1|$ and the entropy, while still extensive, is reduced. Although not marked by a divergent susceptibility, the transition at $T_{\mathrm{SRO}}(p, q)$ is characterized by the development of short-range magnetic order and a reduction in the entropy. Future work may establish connections between the SRO phase and the spin-glass solution to the random Ising model on a Bethe lattice [36], where the Edwards–Anderson order parameter can be explicitly constructed.

The strength of DMFT applied to DE-like models with a Kondo coupling $2J\mathbf{m}_i \cdot \mathbf{s}_i$ between the local-moment spin $\mathbf{S}_i = S\mathbf{m}_i$ and the electron spin $\mathbf{s}_i$ is that the Fermion degrees of freedom in the local action may be integrated exactly, leaving a function only of the local moment direction $\mathbf{m}_i$. Consequently, formally exact results are possible for a range of models where the local moments are treated classically. This stands in stark contrast to the case for the Hubbard model [10], where the action cannot be analytically integrated and quantum Monte Carlo must be used to solve the local problem. We should also mention that the classical treatment of the local spins is more questionable in the manganites, where $S = 3/2$, than in Mn-doped GaAs, where $S = 5/2$.

The discovery of an SRO solution to the DE model in infinite dimensions has wide ramifications. Our results open the door for future studies of the disordered ground-state of the DE model unencumbered by the numerical complexities of Monte Carlo simulations [3] in finite dimensions.

Acknowledgments

It is a pleasure to acknowledge helpful conversations with Professors E Dagotto, J Freericks, D Scalapino and S Yunoki. This research was sponsored by the US Department of Energy under

contract DE-AC05-00OR22725 with Oak Ridge National Laboratory, managed by UT-Battelle, LLC and by the National Science Foundation under Grant Nos. DMR-0073308, DMR-0312680, EPS-0132289 and EPS-0447679 (ND EPSCoR). A portion of this research was conducted at the Center for Nanophase Materials Sciences, which is sponsored at Oak Ridge National Laboratory by the Division of Scientific User Facilities, US Department of Energy.

Appendix A. Weak-coupling results

This appendix presents the weak-coupling results for the SRO transition temperature and energy. For low temperatures, $\sum_n g(\nu_n) \to (1/2\pi T)\int \mathrm{d}\nu\, g(\nu)$ so that

$$T_{\mathrm{SRO}}(p,q) = -\frac{J^2(2q-1)}{3\pi}\int \mathrm{d}\nu \frac{R(\upsilon)}{(\upsilon+R(\upsilon))^2(\upsilon+2(1-q)R(\upsilon)) - J^2(\upsilon+2(2-q)R(\upsilon)/3)}, \tag{A.1}$$

where $\upsilon = \mathrm{i}\nu + \mu$. In the weak-coupling limit $T \ll J \ll W$, this becomes

$$T_{\mathrm{SRO}}(p,q) = -\frac{J^2(2q-1)}{3\pi}\int \mathrm{d}\nu \frac{R(z)}{(z+R(z))^2(z+2(1-q)R(z))}, \tag{A.2}$$

where $z = \mathrm{i}\nu + \mu_0$ and $R(z)$ falls off like W^2/z for large $|z|$. The zeroth-order chemical potential μ_0 is defined in terms of the filling p by equation (56). Using complex analysis and carefully treating the branch cut between $\pm W/2$ along the real axis, we find that

$$\frac{T_{\mathrm{SRO}}(p,q)W}{J^2} = -\frac{32}{3\pi}\int_\delta^1 \mathrm{d}y\, y\sqrt{1-y^2}\frac{y^2-(3-2q)/4}{y^2+b}, \tag{A.3}$$

with $\delta = 2\mu_0/W$ and $b = (1-q)^2/(2q-1)$. Clearly, $T_{\mathrm{SRO}}(p,q)$ vanishes as $q \to 1/2$ or $b \to \infty$.

In the regime $0 \leqslant q \leqslant 1/2$, the integral for $T_{\mathrm{SRO}}(p,q)$ with $b < 0$ gives

$$\begin{aligned}\frac{T_{\mathrm{SRO}}(p,q)W}{J^2} = \frac{8}{9\pi(1-2q)}\Bigg\{&3\sqrt{1-\delta^2} - 4(1-\delta^2)^{3/2}(1-2q) \\ &+\frac{3q}{2\sqrt{1-2q}}\left[\tan^{-1}\left(\frac{(1-q)|\delta|-\sqrt{1-2q}}{\sqrt{1-\delta^2}q}\right) - \tan^{-1}\left(\frac{(1-q)|\delta|+\sqrt{1-2q}}{\sqrt{1-\delta^2}q}\right)\right]\Bigg\}.\end{aligned} \tag{A.4}$$

This result can be extended to the regime $1/2 < q \leqslant 1$ by using the identity

$$\begin{aligned}&\frac{1}{\sqrt{1-2q}}\left[\tan^{-1}\left(\frac{(1-q)|\delta|-\sqrt{1-2q}}{\sqrt{1-\delta^2}q}\right) - \tan^{-1}\left(\frac{(1-q)|\delta|+\sqrt{1-2q}}{\sqrt{1-\delta^2}q}\right)\right] \\ &\qquad = -\frac{2}{\sqrt{2q-1}}\log\left[\frac{q+\sqrt{1-\delta^2}\sqrt{2q-1}}{\sqrt{\delta^2(2q-1)+(1-q)^2}}\right].\end{aligned} \tag{A.5}$$

These expressions yield equation (31) for T_C and equation (36) for T_N as $q \to 0$ and $q \to 1$, respectively.

Using equation (54), it is straightforward to obtain the kinetic energy in the weak-coupling limit:

$$\frac{1}{N}\langle K(p,q)\rangle = \frac{1}{N}E_0(p) + \frac{2J^2}{\pi W(1-2q)}\left\{2\sqrt{1-\delta^2} + \frac{q}{\sqrt{1-2q}}\left[\tan^{-1}\left(\frac{(1-q)|\delta| - \sqrt{1-2q}}{\sqrt{1-\delta^2}q}\right)\right.\right.$$
$$\left.\left. - \tan^{-1}\left(\frac{(1-q)|\delta| + \sqrt{1-2q}}{\sqrt{1-\delta^2}q}\right)\right]\right\}. \tag{A.6}$$

Of course, the NM kinetic energy is obtained by taking the limit $q \to 1/2$, with the result $\langle K(p, q = 1/2)\rangle/N = E_0(p)/N + (16J^2/3\pi W)(1-\delta^2)^{3/2}$. The difference between the q-dependent and NM kinetic energies in the weak-coupling limit is then given by $\Delta\langle K(p,q)\rangle/N = 3T_{SRO}(p,q)/2$.

Likewise, it is straightforward to evaluate the potential energy to order $(J/W)^2$, with the result:

$$\frac{1}{N}\langle V(p,q)\rangle = -\frac{4J^2}{\pi W(1-2q)}\left\{2\sqrt{1-\delta^2} + \frac{q}{\sqrt{1-2q}}\left[\tan^{-1}\left(\frac{(1-q)|\delta| - \sqrt{1-2q}}{\sqrt{1-\delta^2}q}\right)\right.\right.$$
$$\left.\left. - \tan^{-1}\left(\frac{(1-q)|\delta| + \sqrt{1-2q}}{\sqrt{1-\delta^2}q}\right)\right]\right\}. \tag{A.7}$$

In the limit $q \to 1/2$, the NM result is $\langle V(p, q = 1/2)\rangle/N = -(32J^2/3\pi W)(1-\delta^2)^{3/2}$. Hence, the difference between the q-dependent and NM potential energies in the weak-coupling limit is given by $\Delta\langle V(p,q)\rangle/N = -3T_{SRO}(p,q)$. It follows that the change in total energy is given by $\Delta E(p,q)/N = -3T_{SRO}(p,q)/2$, which includes the FM ($q = 0$) and AF ($q = 1$) phases as special cases.

Appendix B. Self-consistency relation for the SRO states

Following the cavity method of [10], the self-consistency relation on the Bethe lattice between the bare and full Green's functions may be written

$$\underline{G}_0(\mathrm{i}\nu_n)^{-1} = z_n \underline{I} - t^2 \sum_i{}' \underline{G}(\mathrm{i}\nu_n)_{ii}, \tag{B.1}$$

where $t^2 = W^2/16z_c$ and $\underline{G}(\mathrm{i}\nu_n)_{ii}$ is the local Green's function on site i. The sum on i is restricted to nearest neighbours of site 0. If the spin on site 0 is aligned along the z axis, then we can write the local Green's function on site 0 as

$$\underline{G}(\mathrm{i}\nu_n)_{00} = \begin{pmatrix} g_{\uparrow n} & 0 \\ 0 & g_{\downarrow n} \end{pmatrix}. \tag{B.2}$$

The creation and destruction operators on site i are taken to refer to a quantization axis that is rotated by angle θ_i (rotation axis in the xy plane at an angle ϕ_i from the x axis) with respect to z. Then $\underline{G}(\mathrm{i}\nu_n)_{ii} = \underline{R}(\theta_i, \phi_i)\,\underline{G}(\mathrm{i}\nu_n)_{00}\,\underline{R}(\theta_i, \phi_i)^\dagger$ is given by

$$\underline{G}(\mathrm{i}\nu_n)_{ii} = \begin{pmatrix} \cos^2(\theta_i/2)g_{\uparrow n} + \sin^2(\theta_i/2)g_{\downarrow n} & \mathrm{i}\sin\theta_i \mathrm{e}^{-\mathrm{i}\phi_i}(g_{\uparrow n} - g_{\downarrow n})/2 \\ -\mathrm{i}\sin\theta_i \mathrm{e}^{\mathrm{i}\phi_i}(g_{\uparrow n} - g_{\downarrow n})/2 & \cos^2(\theta_i/2)g_{\downarrow n} + \sin^2(\theta_i/2)g_{\uparrow n} \end{pmatrix}. \tag{B.3}$$

Summing over all z_c neighbours of site 0 and assuming that ϕ_i is random so that $(1/z_c)$ $\sum_i' \exp(\pm i\phi_i) = 0$, we find

$$\frac{1}{z_c}\sum_i{}' \underline{G}(i\nu_n)_{ii} = (1-q)\begin{pmatrix} g_{\uparrow n} & 0 \\ 0 & g_{\downarrow n}\end{pmatrix} + q\begin{pmatrix} g_{\downarrow n} & 0 \\ 0 & g_{\uparrow n}\end{pmatrix}, \tag{B.4}$$

where $q = (1/z_c)\sum_i' \sin^2(\theta_i/2)$. Upon noting that the two Green's function matrices above are spin-reversed, we obtain equation (46).

Appendix C. Kinetic energy

Previous forms for the kinetic energy utilized the wavevector $\mathbf{q} = 0$ or $\mathbf{Q}$ of the FM or AF phase [10]. In this appendix, we develop an expression for the kinetic energy that also applies to the SRO states, where the wavevector is not defined. Begin with the relation

$$\frac{1}{N}\langle K\rangle = -\frac{t}{2Z_f}\sum_i{}' \int \Pi_i d\Omega_{\mathbf{m}_i} \mathrm{Tr}_f\left((c_{0\alpha}^\dagger c_{i\alpha} + c_{i\alpha}^\dagger c_{0\alpha})e^{-S}\right), \tag{C.1}$$

where $Z_f = \int \Pi_i\, d\Omega_{\mathbf{m}_i} \mathrm{Tr}_f(\exp(-S))$ and the sum over i is restricted to nearest neighbours of site 0. The action $S = \Delta S + S_0 + S^{(0)}$ is separated into terms that involve site 0 and the action $S^{(0)}$ of the cavity [10] with site 0 removed. The kinetic part of the action containing site 0 is

$$\Delta S = -t\int_0^\beta d\tau \sum_j{}' \left(c_{0\alpha}^\dagger(\tau)c_{j\alpha}(\tau) + c_{j\alpha}^\dagger(\tau)c_{0\alpha}(\tau)\right). \tag{C.2}$$

Performing perturbation theory in the term involving the $(0i)$ bond and using $t = W/4\sqrt{z_c}$, we find

$$\begin{aligned}\frac{1}{N}\langle K\rangle &= \frac{W^2}{16 z_c}\sum_i{}' \int_0^\beta d\tau \langle c_{i\alpha}^\dagger(0)c_{i\alpha}(\tau)\rangle\langle c_{0\alpha}^\dagger(\tau)c_{0\alpha}(0)\rangle \\ &= \frac{W^2}{32}T\sum_{l,\eta} G^{(\eta)}(i\nu_l)_{\alpha\beta}\left\{(1-q)G^{(\eta)}(i\nu_l)_{\beta\alpha} + qG^{(\bar\eta)}(i\nu_l)_{\beta\alpha}\right\},\end{aligned} \tag{C.3}$$

where the local averages at sites 0 and i are performed using S_{eff} of equation (2). Removing the single $(0i)$ bond from ΔS does not affect those local averages in the $z_c \to \infty$ limit.

References

[1] For an overview of work on the manganites, see Dagotto E 2003 *Nanoscale Phase Separation and Colossal Magnetoresistance* (Berlin: Springer)
Dagotto E 1999 *Physics of Manganites* ed T A Kaplan and S D Mahanti (New York: Plenum)
[2] For an overview of work on dilute magnetic semiconductors, see MacDonald A H, Schiffer P and Samarth N 2005 *Nat. Mat.* **4** 195
Dietl T 2003 *Advances in Solid State Physics* ed B Kramer (Berlin: Springer) (*Preprint* cond-mat 0306479)
[3] Yunoki S, Hu J, Malvezzi A L, Moreo A, Furukawa N and Dagotto E 1998 *Phys. Rev. Lett.* **80** 845
Dagotto E, Yunoki S, Malvezzi A L, Moreo A, Hu J, Capponi S, Poilblanc D and Furukawa N 1998 *Phys. Rev.* B **58** 6414
[4] Nagai K, Momoi T and Kubo K 2000 *J. Phys. Soc. Japan* **69** 1837

[5] Chattopadhyay A, Millis A J and Sarma S D 2000 *Phys. Rev.* B **61** 10738
Chattopadhyay A, Sarma S D and Millis A J 2001 *Phys. Rev. Lett.* **87** 227202
Chattopadhyay A, Millis A J and Sarma S D 2001 *Phys. Rev.* B **64** 012416
[6] Yin L 2003 *Phys. Rev.* B **68** 104433
[7] Van Vleck J H 1962 *Rev. Mod. Phys.* **34** 681
[8] Müller-Hartmann E 1989 *Z. Phys.* B **74** 507
Müller-Hartmann E 1989 *Z. Phys.* B **76** 211
[9] Metzner W and Vollhardt D 1989 *Phys. Rev. Lett.* **62** 324
[10] For a review of DMFT, see Georges A, Kotliar G, Krauth W and Rozenberg M J 1996 *Rev. Mod. Phys.* **68** 13
[11] Furukawa N 1995 *J. Phys. Soc. Japan* **64** 2754
Furukawa N 1995 *J. Phys. Soc. Japan* **64** 3164
[12] Millis A J, Mueller R and Shraiman B I 1996 *Phys. Rev.* B **54** 5389
Millis A J, Mueller R and Shraiman B I 1996 *Phys. Rev.* B **54** 5405
Michaelis B and Millis A J 2003 *Phys. Rev.* B **68** 115111
[13] Furukawa N 1999 *Physics of Manganites* ed T A Kaplan and S D Mahanti (New York: Plenum)
[14] Auslender M and Kogan E 2001 *Phys. Rev.* B **65** 012408
Auslender M and Kogan E 2002 *Europhys. Lett.* **59** 277
Auslender M and Kogan E 2003 *Phys. Rev.* B **67** 132410
Kogan E, Auslender M and Dgani E 2002 *Preprint* cond-mat 0211354
[15] Fishman R S and Jarrell M 2003 *J. Appl. Phys.* **93** 7148
Fishman R S and Jarrell M 2003 *Phys. Rev.* B **67** 100403(R)
[16] Chernyshev A and Fishman R S 2003 *Phys. Rev. Lett.* **90** 177202
[17] Fishman R S, Maier Th, Moreno J and Jarrell M 2005 *Phys. Rev.* B **71** 180405(R)
[18] Aryanpour K, Moreno J, Jarrell M and Fishman R S 2005 *Phys. Rev.* B **72** 045343
[19] Brinkman W F and Rice T M 1970 *Phys. Rev.* B **2** 1324
[20] Fishman R S, Popescu F, Alvarez G, Moreno J and Maier Th 2006 *Phys. Rev.* B **73** 140405(R)
[21] Binder K and Young A P 1986 *Rev. Mod. Phys.* **58** 801
[22] Baym G and Kadanoff L P 1961 *Phys. Rev.* **124** 287
Baym G 1962 *Phys. Rev.* **127** 1391
[23] Jarrell M 1992 *Phys. Rev. Lett.* **69** 168
[24] Freericks J K and Jarrell M 1995 *Phys. Rev. Lett.* **74** 186
[25] Bickers N E 1987 *Rev. Mod. Phys.* **59** 845
[26] Leath P L 1968 *Phys. Rev.* **171** 725
[27] For a general reference, see Abrikosov A A, Gorkov L P and Dzyaloshinski I E 1963 *Methods of Quantum Field Theory in Statistical Mechanics* (Englewood Cliffs, NJ: Prentice-Hall)
[28] Nolting W, Rex S and Mathi Jaya S 1997 *J. Phys.: Condens Matter* **9** 1301
[29] Santos C and Nolting W 2002 *Phys. Rev.* B **65** 144419
Santos C and Nolting W 2002 *Phys. Rev.* B **66** 019901
[30] Trias A and Yndurain F 1983 *Phys. Rev.* B **28** 2839
[31] Rogan J and Kiwi M 1997 *Phys. Rev.* B **55** 14397
[32] Gruber Ch, Macris N, Royer Ph and Freericks J K 2001 *Phys. Rev.* B **63** 165111
[33] Eggarter T P 1974 *Phys. Rev.* B **9** 2989
[34] Bitko D, Coppersmith S N, Leheny R L, Menon N, Nagel S R and Rosenbaum T F 1997 *J. Res. Natl Inst. Stand. Technol.* **102** 207
[35] Schmalian J and Wolynes P G 2000 *Phys. Rev. Lett.* **85** 836
[36] Bowman D R and Levin K 1982 *Phys. Rev.* B **25** 3438
Thouless D J 1986 *Phys. Rev. Lett.* **56** 1082
de Oliviera M J 1989 *J. Phys. A: Math. Gen.* **22** 4433